Australian Government

Murray–Darling Water & Environment Research

Forecasting risks to fish and their available habitat from low flows and hypoxia

Final report

September 2024

Forecasting risks to fish and their available habitat from low flows and hypoxia

Report prepared by:

Ryan Shojinaga and David P. Hamilton

Australian Rivers Institute, Griffith University, Brisbane

For:

MD-WERP Theme 3, Research Question 9.2: Forecasting risks to fish and their available habitat from low flows and hypoxia

September 2024

Author contact details

☏ +61 429 395 041

✉ ryan.shojinaga@griffith.edu.au

✉ david.p.hamilton@griffith.edu.au

https://www.griffith.edu.au/australian-rivers-institute

Report citation

Shojinaga R., Hamilton, D. P. 2024. MD-WERP Theme 3, Research Question 9.2: Forecasting risks to fish and their available habitat from low flows and hypoxia. ARI Report No. 2024/008. Australian Rivers Institute, Griffith University, Brisbane

Executive Summary

The rivers and streams of the Murray-Darling Basin (MDB) frequently experience little or no flow. During these times, the threats to native fish are heightened due to the potential for poor water quality to diminish habitat availability and quality. Hypoxia and anoxia, corresponding to low or no oxygen in the water column, respectively, pose some of the greatest risks to fish survival. Fish rely on specific ranges of dissolved oxygen (DO) in the water column to survive. When suitable habitat diminishes or disappears, fish kills can occur, including recently in the summers of 2018-2019 and 2023 in the Darling River at Menindee.

Poor water quality, which includes conditions of hypoxia and anoxia, is a result of many in-stream, near stream, regional and global factors, such as flow conditions, elevated nutrients and sediment in runoff, or the local weather. The degree to which any of these factors has an impact is complex, affected by multiple different drivers, and often specific to a waterbody.

This report presents research aimed at identifying many of these factors in the context of the dryland rivers of the MDB and quantifying the potential risks or benefits they pose to water quality and fish habitat. Specifically, we evaluated water quality conditions and contextual factors in two river reaches, one a persistent, isolated waterhole on the Culgoa River, and the other a flowing, regulated waterway—the Darling River at Menindee Lakes.

Our analysis was supported by the creation of a three-dimensional (3D) hydrodynamic and water quality model of each reach, executing those models under a range of conditions, and analysing the results using metrics that relate to habitat or conditions that have implications for habitat. We then used the results from these analyses to evaluate the importance of local, regional, and global factors on water quality in the MDB. The three broad groups of factors considered in this report are climate, riparian vegetation and flow.

We found that global factors (climate change), have the potential to create some of the worst conditions for water quality. Warmer air temperatures under a range of climate change scenarios create warmer water temperatures, resulting in some of the lowest DO concentrations, even under modest climate change predictions. Stratification, broadly indicated by the difference in surface and bottom temperatures, is a risk factor for low-oxygen or no-oxygen conditions. Climate change is predicted to increase stratification and resistance of the water column to mixing by wind or flow, compared to any direct effects from changes in riparian vegetation and flow. Climate change has the potential to reduce fish habitat for vulnerable species to less than half of the total waterhole volume by the end for the period of modelling simulations presented in this report.

Flow also has profound impacts on water quality and risks to fish in the MDB. We found that flows introduced to isolated waterholes (Culgoa River) as a means of refreshing or resetting water quality can introduce oxygenated water and increase DO over the base flow conditions, however, higher turbidity from scour and resuspension might inhibit productivity while lower metalimnetic (mid-water) and hypolimnetic (bottom-water) temperatures from deeper, more turbid water might create greater stratification and lower DO concentrations, resulting in greater overall risk to fish viability. When a river is already flowing (Darling River), low flows create the greatest intensity of stratification and depress DO most, especially in the mid (metalimnion) and bottom (hypolimnion) waters. Conversely, we found high flows elevate DO and temperature throughout the water column, while decreasing stratification.

Changes in riparian vegetation and flow were used in the scenarios as a means of exploring possible management lever to mitigate conditions that would lead to fish kills. Our study found that riparian vegetation is important, however results are mixed in terms of exacerbating or mitigating the risks to fish. At the isolated waterhole (Culgoa River), the modelling showed that clearing vegetation would increase wind exposure and decrease the intensity of stratification. The reduced riparian vegetation would increase solar radiation at the surface of the water, enhancing productivity. The resulting increase in absorption of solar radiation from the elevated biomass at the surface was a driver for the decrease in water temperatures deeper in the water column, although it would increase temperature in surface waters. Clearing of riparian vegetation adjacent to the streambank reduced stratification. The effects of altering riparian vegetation should be considered carefully as they can have other water quality impacts not included within the scope of this report. For flowing conditions (Darling River) changes in riparian vegetation did not result in significantly different water quality conditions over base conditions, likely due to limits of the relative size of river (width) and amount of shading the vegetation was capable of providing.

Finally, we examined the degree to which many of the system variables changed in relation to one another. These variables included geomorphology (i.e., channel geometry), riparian vegetation, climate, hydrodynamics, water quality, stratification, and habitat. We examined correlations between indicators (e.g., vegetation height) and response variables (e.g., DO concentrations). In addition to supporting the findings arising from the scenarios, these analyses showed that many water quality and habitat variables respond in diverging ways to environmental conditions, whether observed in the waterhole or in the flowing river. For example, DO concentration increases as width and depth increase in the isolated waterhole (Culgoa River), but decrease with increasing width and depth in flowing conditions (Darling River). Some of the strongest associations were between water temperature and air temperature; DO and air temperature; and fish habitat and DO concentrations. The strong interrelationships among these variables demonstrate the value of using a coupled hydrodynamic-ecological model capable of integrating forcing variables (e.g., climate, flow) with the internal ecological processes in the river.

The results presented in this report highlight the need to prioritise management strategies to optimise water quality conditions and preserve fish habitat. Temperature and DO are critical parameters for optimising water quality, but both can be expected to be altered by changing climate, almost certainly in negative ways that will necessitate vigilant management. This report has presented how water quality may be altered under different scenarios , as well as strategies to counteract those changes. While we have endeavoured to evaluate water quality in the MDB under a broad range of conditions, our study could not consider all conditions. We acknowledge our data sets and analyses may not be comprehensive; however, we present this report and the sophisticated tools herein as a step forward in understanding the risks and opportunities in protecting the valuable resources in the Murray-Darling Basin.

Table of contents

List of Tables

Figure captions

Introduction

Background

The Murray–Darling Water and Environment Research Program (MD-WERP) is designed to improve knowledge of the Murray–Darling Basin and support Basin management by examining climate adaptation and hydrology in the Basin, and predicting the resulting environmental, social, economic and cultural outcomes. The MD-WERP program started in 2019 and has a 4-year duration, including working with Commonwealth partners: the Department of Climate Change, Energy, the Environment and Water, the Commonwealth Environmental Water Holder, and the Murray–Darling Basin Authority. Theme 3 of the MD-WERP has been undertaken by a consortium of Griffith University, La Trobe University and the Murray Lower Darling Rivers Indigenous Nations. Here we provide a summary report on Research Question 9.2: Forecasting risks to fish and their available habitat from low flows and hypoxia. This summary report contains key model simulation outputs and their interpretation, and a fact sheet (Deliverable Code 9.2.1).

In 2021 researchers, water policy and water managers, along with First Nations advisors, co-designed the research program to help ensure the research met the needs of the end users. Dryland rivers are critical to supporting wildlife in the arid tropics and subtropics of Australia (*Figure 1*). Species have adapted to the 'boom and bust' cycles of non-perennial (intermittent) rivers, sustained by refugia and transient food webs in both flowing channels and isolated waterholes. These food webs rely on not only the supply of water but also sufficient oxygen to thrive. Pressure from global change reduces waterhole viability and reliability by changing water quantity and quality and depleting available oxygen in the water column for biota to live (Bunn et al., 2006). Such conditions, referred to as hypoxia, are deleterious to ecosystems and biodiversity (Beavis et al., 2023), while complete loss of oxygen (anoxia) results in further deleterious chemical changes (Hou et al. 2013).

Figure 1. Moonie River in the Murray-Darling Basin, Australia, showing a waterhole and part of the dry river channel. These waterholes are important for biodiversity and people in dryland river regions. Photo provided by Jonathan Marshall (Dept of Environment and Science, Queensland Govt, Australia, n.d.).

Riparian zones are ecotones between the landscape and stream ecosystems. They are terrestrial biomes with functional impacts for the streams they border. These functions, which include buffering environmental conditions, help regulate the internal (e.g., in-river) state (Anbumozhi et al., 2005; Sweeney & Newbold, 2014). For example, riparian vegetation has been shown to reduce water temperature and productivity of plants and algae by blocking incident solar radiation (Rutherford et al., 1997). While not affecting oxygen directly, the loss of riparian vegetation has been linked with increased water temperatures and altered dissolved oxygen regimes (Bernot et al., 2010). Furthermore, riparian vegetation alters wind speed at the water surface (Zhai et al., 2023), and supplies organic matter to the stream, both of which impact water quality and dissolved oxygen.

Our understanding of the connections between global, regional, and local conditions and their influence on water quality conditions in the Murray-Darling Basin is incomplete. For example, how do aspect and vegetation height affect weather at the local scale? How does the resulting microclimate affect water quality and fish habitat? These kinds of inquiries underpin two general questions: (1) how will fish habitat change in response to changing climate, and (2) how can we manage and mitigate the risks associated with those changes?

To aid in our understanding of drivers of poorly oxygenated or anoxic waters in isolated waterholes and dryland rivers in the arid and semi-arid subtropics, we have developed an integrated model linking climate and hydrology with riparian vegetation and water quality. The model allows us to investigate how the riparian structures in dryland rivers of the Murray-Darling Basin (MDB) affect temperature and dissolved oxygen. The model also allows us to study how flow and nutrients can intensify or alleviate the risks of poor water quality, and unsuitable conditions for fish.

Preliminary study

In 2022, the Queensland Government, with several partner organisations, published a report titled 'Between a hot place and hypoxia: Modelling fish-kill risk in Queensland waterholes' (Zhai et al., 2022). That study (referred to henceforth as HPH) provided detail on how isolated waterhole conditions contributed to risks of hypoxia and fish-kills. The study included modelling of water quality of 6 waterholes in the northern Murray-Darling Basin and used the water quality model to develop indices of suitable and unsuitable conditions for 4 fish species. Some of the key findings of the study included how conditions are often site-specific, with risk thresholds linked to critical water levels and environmental conditions at sites. The study also identified the need for more detailed modelling to understand local conditions and micro-climate effects on water quality.

Our intent is to build upon the HPH study, expounding upon the significance of local conditions and effects on water quality and the risk of hypoxia. Our study expands the resolution of the modelling to better understand how conditions in both space and time contribute to or mitigate the risk of hypoxia. The extended resolution includes the specification of riparian conditions throughout the domain of the model; looking at water quality in multiple dimensions; differences in flowing vs. non-flowing reaches; and incorporating more processes into water quality dynamics. Specifically, the work extends the HPH study by looking at the impacts of multiple stressors on water quality in a range of contexts.

Using these added dimensional elements and increased resolution, the overall objective of this component of the study is:

- To carry out a risk assessment of local, regional and global factors affecting temperature and dissolved oxygen, and affecting fish distributions. This risk assessment is supported by model simulations that will ultimately consider the relevant mitigation and management strategies to improve habitat for fish in the Murray-Darling system and alleviate risks of fish kills.

Methods

Study reaches

We have modelled two study areas which present different challenges to water quality and fish health, but also different opportunities to learn from. In the first study reach, we examine a relatively small, isolated waterhole that remains disconnected from the flowing river for several months, and in the second study reach we examine a large flowing river that has experienced recent significant water quality issues, including fish die-off events.

Culgoa River at Brenda Weirpool

Our first study reach is on the Culgoa River (SR1), a 435-km river that begins where the Balonne River splits near Dirranbandi, becoming the Culgoa River and the eastern branch of the Balonne River. The Culgoa River drains a basin of 90,000 sq. km[1] and merges with the Barwon River, the continuation of the East Fork Balonne River, to form the Darling River (Figure 2).

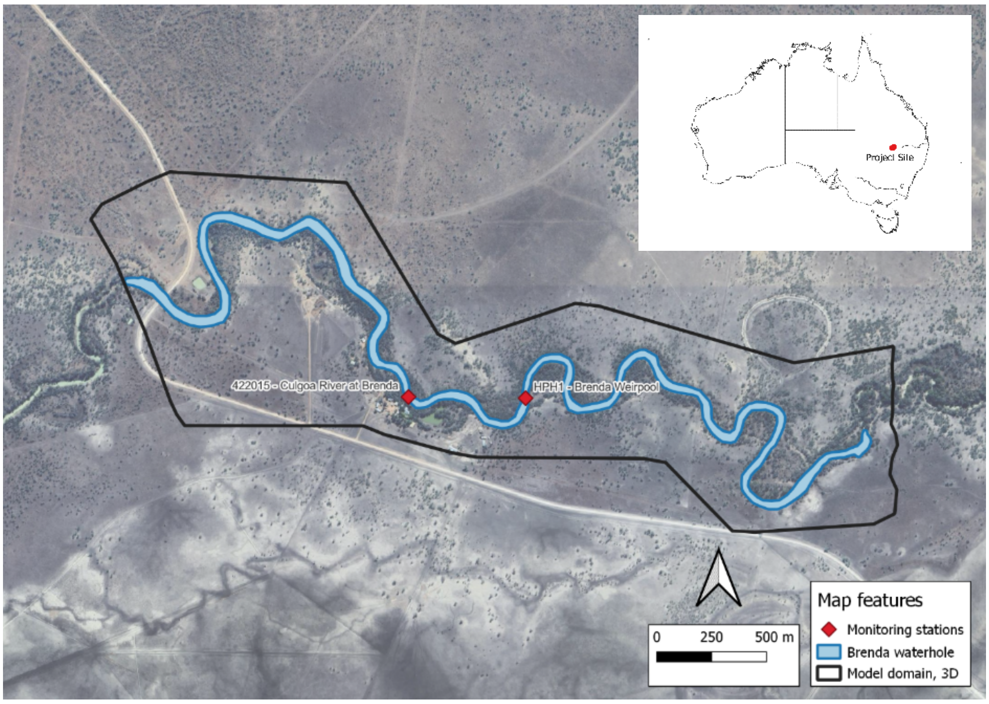

Figure 2. Study area 1 of the Culgoa River at Brenda weir pool, including model domain (black line), HPH model domain (blue area), and HPH monitoring chain and WaterNSW flow gauge locations (red diamonds).

The Culgoa basin is generally subject to a semi-arid climate, especially in the lowland reaches. The rivers and streams are generally non-perennial and regularly have periods of drought and floods. In Queensland the Culgoa River is within the Condamine-Balonne Surface Water Management Plan (DNRME, 2019), which includes larger storages of Beardmore Dam on the Balonne River (82 GL) and Leslie Dam on the Upper Condamine (106 GL); and smaller storages of Jack Taylor Weir on the Balonne River (10 GL) and the Chinchilla Weir on the Condamine River (10 GL) (BOM)[2]

Land use within the basin is primarily rangeland with some dryland and irrigated agriculture. Forested areas are present in the upper regions of the catchment. The basin is entirely within the Great Artesian Basin. Bioregions of the basin include the Brigalow Belt, Mulga Lands, New England Tableland, and

---

[1] https://wetlandinfo.des.qld.gov.au/wetlands/facts-maps/water-resource-planning-area-condamine-and-balonne/

[2] http://www.bom.gov.au/water/nwa/2020/mdb/regiondescription/geographicinformation.shtml

Southeast Queensland (SEQ). The population within the basin is approximately 57,000 comprised within towns such as Toowoomba, Warwick, Roma, Chinchilla, and Miles, and is mostly located within the upper regions of the catchment.

The study area is a reach of approximately 3.5 km in the middle Culgoa River, at the Brenda weir pool, where the Brenda (422015[3]) gauge has been used to actively report flow since 1960. The mean annual flow volume at 422015 is 400 gigalitres per year. Peak daily flow was 1166 $m^3 s^{-1}$ (in 2012) for gauge 422015. The gauge at Brenda (422015) has experienced zero flow 40 percent of the time during its period of record (i.e., no flows are observed 40 out of every 100 days on average).

The average streambed slope in the study reach is 0.15 m per 1.0 km. The Culgoa flows through plains of cracking grey and brown clays with areas of gilgais (wetlands caused by contracting and expanding clays) from historical flow patterns. Some alluvial substrates are associated with flow channels of present-day and the more recent past.

Darling River at Menindee Lakes

The Darling River at Menindee Lakes has been the subject of intense interest related to water quality, drought, overall-allocation, and fish kill events. The Darling River in this area has historically flowed even in droughts, though upstream water use is changing the hydrology (Mallen-Cooper & Zampatti, 2020). The Darling River is experiencing increased low and no-flow events, likely as a result of increased water extraction (Durrant-Whyte, 2023).

Fish kills in 2018-2019 and 2023, have demonstrated the need for improved understanding of water quality dynamics and robust tools within this system (Vertessy et al., 2019; Sheldon et al., 2022). An inquiry into the 2018-2019 fish kills found that low flow and water stagnation elevated productivity, and variable climatic conditions caused the fish kills. To address these issues and their contextual precursors, Vertessy et al. (2019) recommended additional monitoring to facilitate a better understanding of the system from a holistic perspective. In 2023, WaterNSW installed more monitoring stations to capture vital information relating to dissolved oxygen (DO) and water temperature in the Darling River at Menindee. These data are made publicly available through their website[4].

The second study reach on the Darling River at Menindee Lakes (SR2) makes use of the data that has been captured thus far, however short in duration. We modelled the Darling River at Menindee from the Menindee Main Weir to Weir 32. This study reach is 41 km long and approximately 600 km downstream of SR1. The Darling River drains 575,000 km^2, including the Culgoa River, eventually merging with the River Murray ~225 km downstream (Figure 3).

The system in this area includes two upstream inflows from Pamamaroo Lake (425995) and Menindee Main Weir (425997). Immediately downstream of Menindee Main Weir the flow gauge 425034 records continuous water level, flow and temperature. Another inflow to the system occurs from Menindee Lake (425994) downstream of the Menindee Town. At the downstream end of the study river reach, is a flow gauge (Weir 32; 425012) that records water level, flow, temperature, and DO at fixed intervals continuously. Two temperature and DO stations were installed at the end of 2023 to record continuous temperature and DO at depths of 0.75, 2 and 3 m (42510101 and 42510102), while a gauge at Menindee Town (425001) records temperature and DO (from 23/03/2023), as well as water level at fixed intervals continuously (from 01/01/1881).

[3] https://realtimedata.waternsw.com.au/water.stm
[4] https://waterinsights.waternsw.com.au/

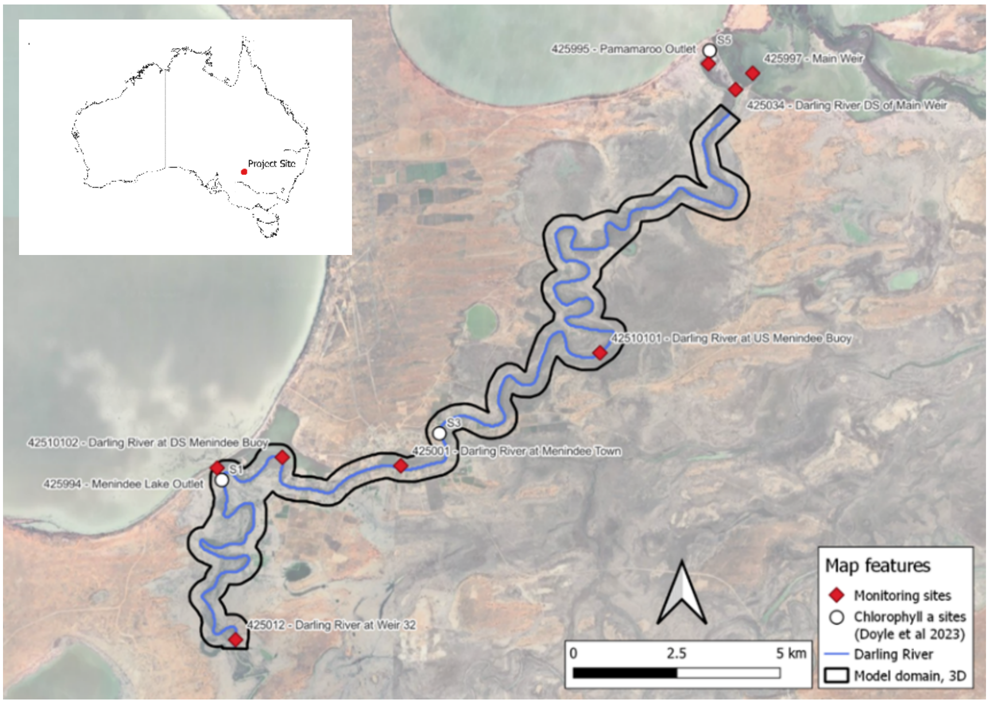

Figure 3. Study area 1 of the Darling River (thick blue line) at Menindee Lakes, including model domain (black line), and monitoring locations (red points).

Data collection and sources

Water quality modelling typically requires datasets to force a set of environmental boundary conditions in space and time within the modelling domain. These conditions might include weather, such as air temperature, mass transfer, such as stream flow into or out of the model domain, and physical conditions such as stream morphology or riparian vegetation presence or absence. Initial conditions and model parameters also make use of these datasets. The nature and source of the data used to construct the models described in this report are discussed in this section, and the subsequent section discusses how the datasets are employed to create boundary conditions, initial conditions, and model parameters.

Water quality

Primary water quality data consisted of continuous DO and temperature data for the study reaches. Continuous DO and temperature data were used to calibrate the models by fitting modelled outputs to the historical time series of these datasets, including profiles within the water column.

Culgoa River

For SR1, continuous temperature and DO data at depths from the HPH project were used as the primary water quality data set. The data from that project consisted of monitoring chains deployed at several dryland waterholes to construct one-dimensional water quality models. The monitoring chains collected temperature and dissolved oxygen data at depths of regular intervals for several months (Figure 4). The HPH report can be referred to for further details about the data, including the data collection process. Only data for the Brenda weir pool were used for this study, and the period of collection was from 28/08/2019 to 05/03/2020; a period of 6 months.

Darling River

For SR2, the primary water quality datasets included continuous temperature and DO data from the state of New South Wales. There are two stations (42510101 and 42510102; Figure 4) that record temperature and DO at three depths in the water column, located in the middle of the reach.

Temperature and DO are also collected at a single depth at three other station (425034, 425001 and 425012). The modelling timeframe for Menindee Lakes started 01/07/2023 to 28/04/2024 for model calibration.

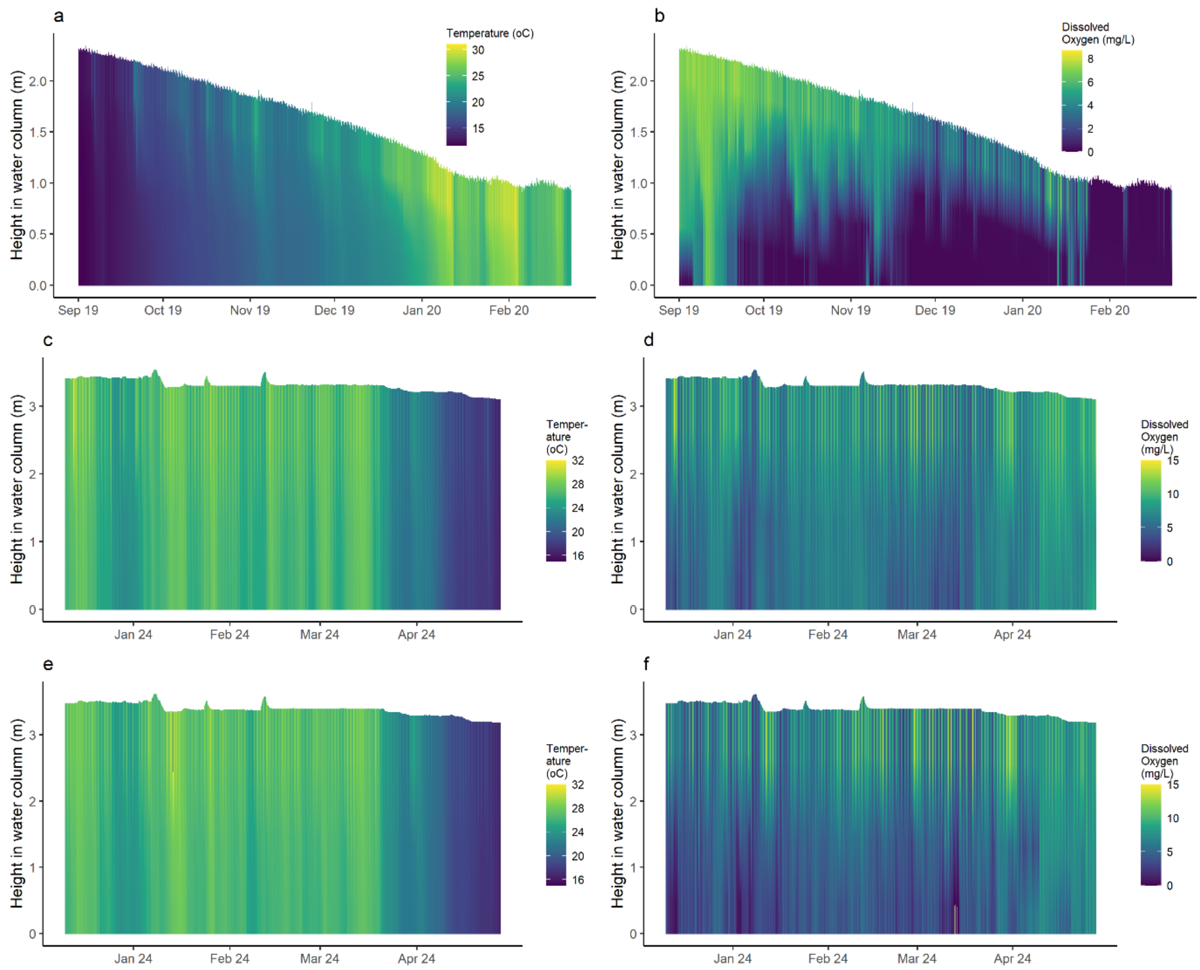

Figure 4. Primary water quality data as a function of time and depth for study sites: (a) Culgoa River temperature at Brenda Weirpool, (b) Culgoa River DO at Brenda Weirpool, (c) Darling River temperature at site 42510101 (d), Darling River DO at site 42510101 (e) Darling River temperature at site 42510102, and (f) Darling River DO at site 42510102.

Point cloud and LiDAR data

A crucial element to building the model is the characterization of riparian vegetation in order to accurately simulate spatially explicit solar radiation and wind data. We used point cloud data collected as part of the LiDAR Upper Darling 2013-2014 project (Geoscience Australia, 2014) for the Culgoa River and the Menindee Lower Darling 2019 project (Geoscience Australia, 2019) for the Darling River at Menindee to derive the physical properties of the riparian vegetation, such as canopy height and density, as well as bare earth ground elevations and potential locations of persistent waterholes (Figure 5).

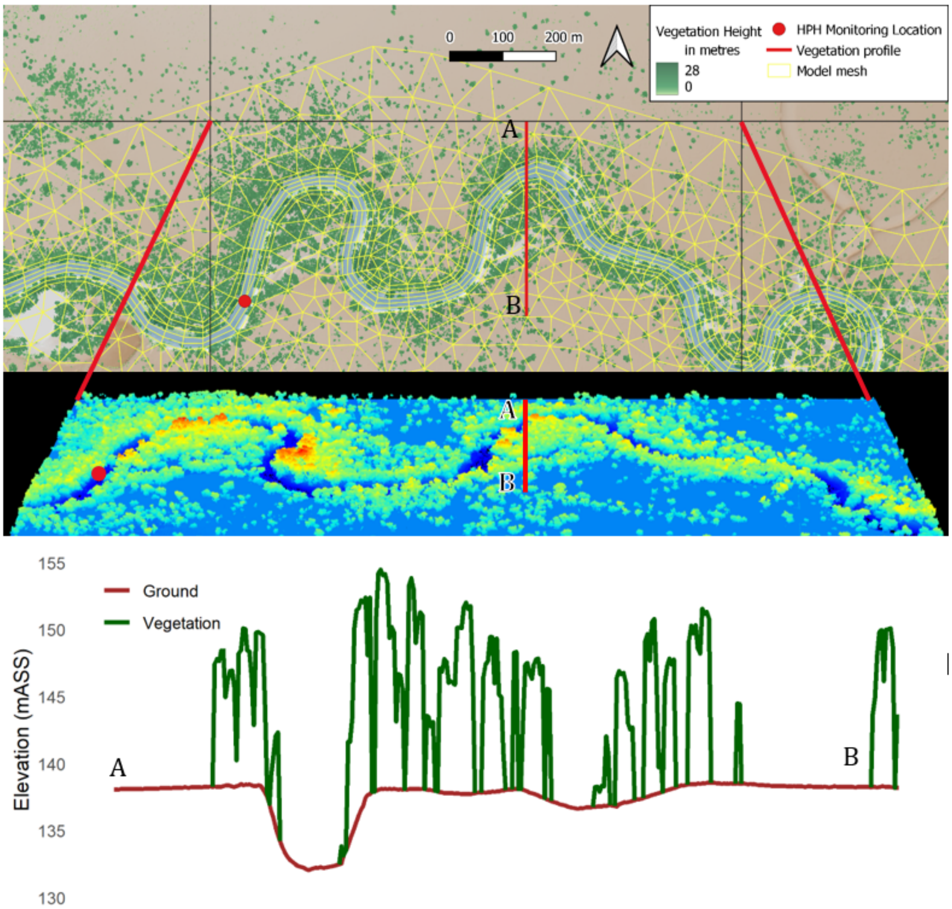

Figure 5. Multiple views of riparian vegetation along the Culgoa River at the HPH monitoring chain location (red dot). The top panel is a plan view, also showing the model grid overlaying the vegetation heights; the middle panel shows a three-dimensional (3D) render of the vegetation from an oblique angle and the bottom panel shows a profile view from downstream to upstream. The letters A and B show the locations of the vegetation profile section in each figure.

Additional data

In addition to the main sources of data described above, we obtained other data, such as flow gauges, water quality, bathymetry and meteorological data from publicly available sources. We describe below the different data types, their source, and how they were used in the model in the subsequent sections where relevant.

Model configuration and construction

There are two main components of the model, the riparian vegetation model derived from the point cloud data and the in-stream water quality model. The riparian vegetation model was used to simulate the terrestrial components of near-stream weather and organic matter inputs to the stream, and the water quality model is used to simulate the effects of those components on water quality, particularly temperature and dissolved oxygen. With these inputs, the modelling workflow progressed from characterising the riparian vegetation, to quantifying its localised effects on solar radiation, air temperature, and wind conditions and using the input data as boundary conditions to construct and execute the water quality models (Figure 6).

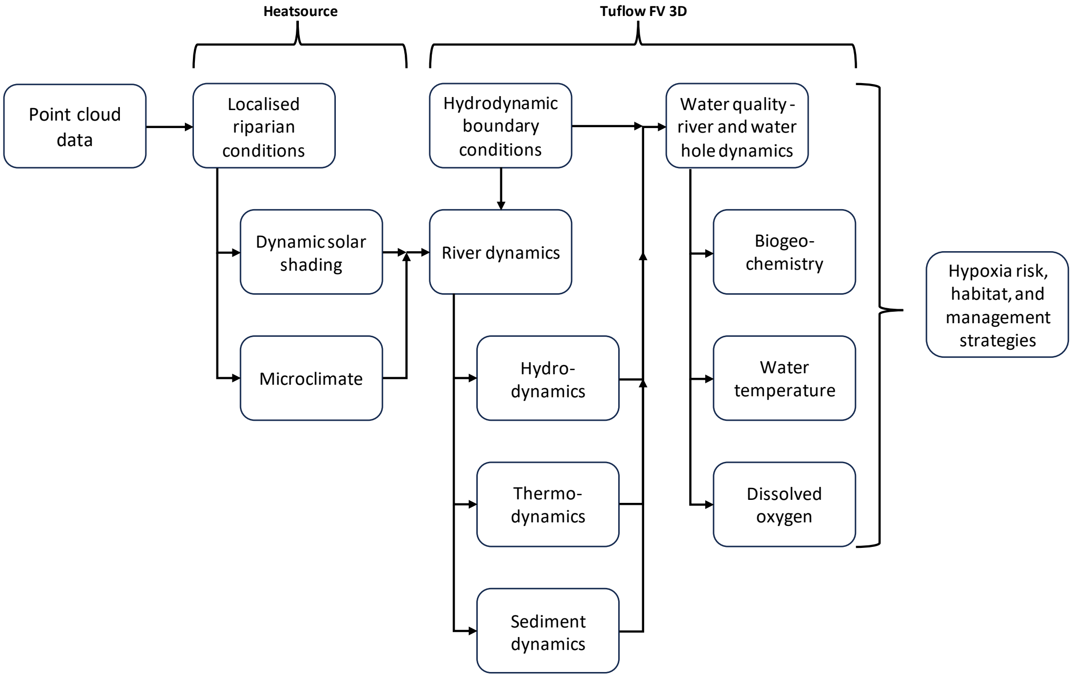

Figure 6. Modelling process description and workflow showing the major components of each step.

We selected the Heatsource model (Boyd & Kasper, 2003) to dynamically simulate the effects of the vegetation on the solar radiation. Heatsource is a stream temperature simulation model that continuously samples riparian vegetation along the length of the model domain and calculates solar shading and the radiation that occurs at the stream surface. Heatsource has been used extensively in the United States for scientific and regulatory purposes. The main input to the Heatsource model is the point cloud characterisation of the riparian vegetation in terms of vegetation height and density.

For modelling in-stream water quality, we selected Tuflow FV (Tuflow; BMT, 2023a, 2023b). Tuflow is a dynamic finite volume model that simulates hydrodynamics, atmospheric heat exchange, sediment transport and biogeochemistry within all types of waterways. Tuflow employs a flexible mesh scheme for fitting the model to the physical features of the waterway, and can be run in 1, 2 and 3 dimensions. Solar radiation, air temperature, and wind conditions based on the riparian vegetation model are used within the Tuflow model to simulate thermodynamics, biogeochemistry and primary production, each of which impact DO and water quality. Tuflow modelling for this project was conducted in three dimensions (3D) to simulate stratification and the full biogeochemical dynamics within the water column. The Tuflow water quality module consists of several interconnected subcomponents, which require proper parameterization to affect a suitable model:

- Atmospheric flux, including gas pressure equilibria for DO, CO_2, N_2, and water vapor.
- Inorganic and organic processes, such as nutrient and carbon cycling. This include s individual partitions of nutrients from inorganic and organic forms (e.g., nitrate) to labile and refractory forms (e.g., dissolved particulate phosphorus; see Calibration *evaluation table 1)*
- Benthic fluxes, such as sediment oxygen demand.
- Phytoplankton (e.g. algae) that underpins water column primary productivity.

We used a suite of quantitative and qualitative calibration metrics to assess the performance of the model. We performed all evaluations for the 2D modelled parameters of flow, water level, and for the 3D modelled parameters of temperature and dissolved oxygen. We did not perform calibration for the Heatsource model shade outputs, because we did not have field data for shading or solar input.

Model domain and mesh

Culgoa River

SR1 consisted of the Brenda weir pool on the Culgoa River from the weir to upstream approximately 3.5 km. The main channel of the Culgoa River within the mesh was typically represented by 4-6 quadrilaterals across at bankfull discharge. Some side channels were represented by quadrilateral cells, and the remainder of the model domain was represented by triangular cells of varying size (Figure 7). Overall, the model mesh consists of more than 2700 2D cells, and almost 9300 3D cells.

The 3D vertical configuration consists of 16 z (vertical) layers and 3 sigma layers. The z layers were of fixed elevation and thickness (0.125 m) from 130.25 to 132.25 meters above mean sea level (m asl). Sigma layers sit on top of the z layers and vary in thickness depending on the water level. The HPH project can be consulted for highly resolved vertical resolution of isolated waterholes. While vertical layers vary with depth, the horizontal dimensions of the vertical cells remain the same. Bathymetry of the Culgoa River at Brenda was surveyed using a boat mounted sonographic device to accurately portray features under the water as part of the first phase of the HPH. These bathymetric data were used to establish elevations of cells and cell vertices in the model.

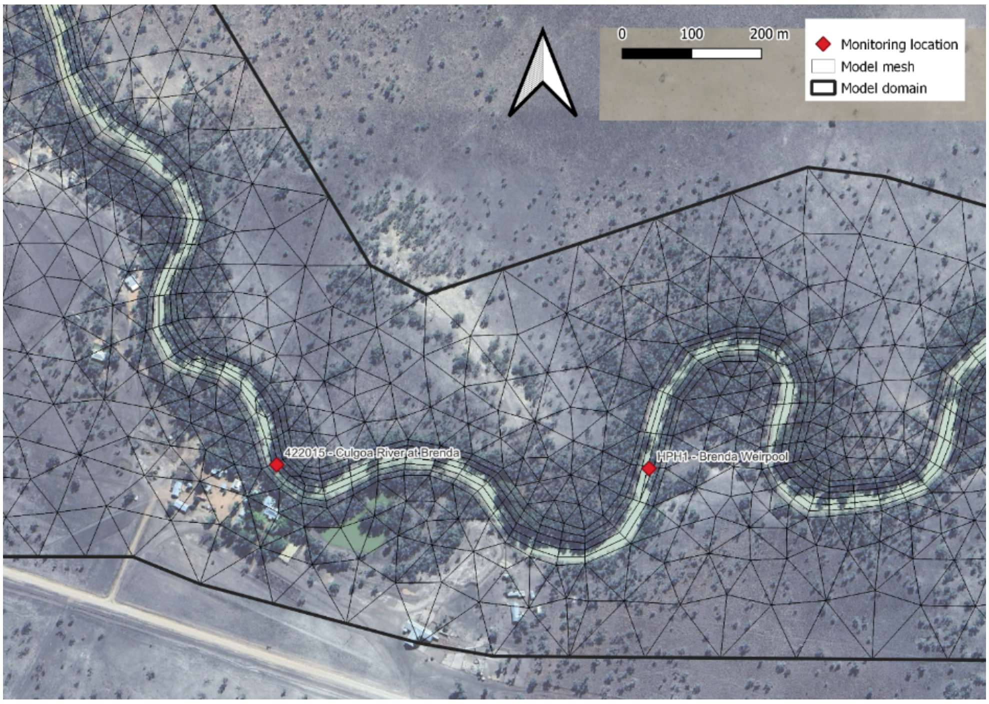

Figure 7. Example of the flexible Tuflow FV model mesh at the Brenda Weir pool, showing the HPH monitoring chain location.

Darling River

The model for the Darling River begins 600 m downstream of Menindee Main Dam and follows the channel of the Darling to just upstream of Weir 32. The lateral width included approximately 300 m on either side of the river and included the area where Menindee Lake discharges to the Darling River (Figure 8).

The main channel of the Darling River was represented by 3-4 quadrilaterals across at bankfull discharge. Overall, the model mesh consists of approximately 8600 2D cells and more than 20,000 3D cells. The vertical configuration of the model on the Darling consists of 10 z layers of 0.50 m thickness from 48.0 m to 53.0 m asl, and 2 sigma layers.

For the Darling River at Menindee Lakes, we used a combination of sources to derive bathymetry, including flow gauges (details provided by WaterNSW), and bathymetry from the Darling River Flood Mapping Study (Manly Hydraulics Laboratory, 2023).

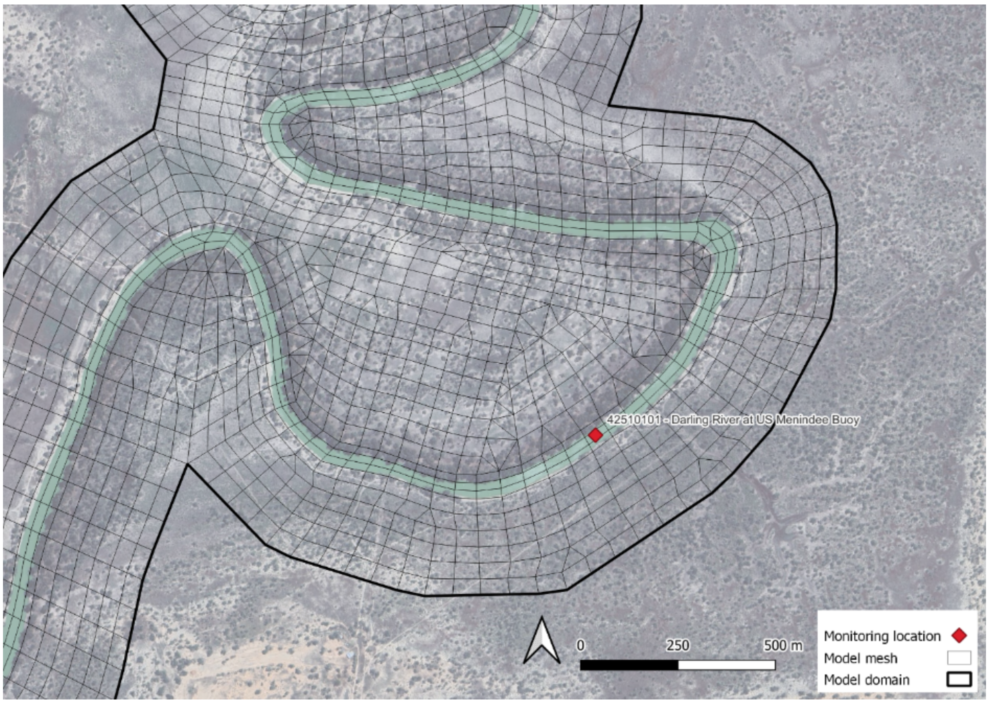

Figure 8. Example of the flexible Tuflow FV model mesh on the Darling River at DO/temperature sensor 42510101.

Modelling time frames

Culgoa River

We selected model calibration time frames based around the HPH water quality data time frame from 28/08/2019 to 05/03/2020. We truncated this period to the beginning of 01/09/2019, to 18/02/2020. Large flow events occurred at the end of February and beginning of March 2020 that we did not calibrate the no-flow model simulation period to. Water levels at the Brenda flow gauge (422015) were available throughout the modelled timeframes.

Darling River

For the Darling River, we selected model calibration time frames based on the availability of DO and temperature data from the upstream gauge (425034). That gauge began collecting DO data on 15/06/2023. The modelling period started at 01/07/2023 and extended the period through to 28/04/2024, when model construction began. The gauges within the model domain have data for at least a portion of the modelling phase, and the gauges at the boundaries have data for the entire modelling period. The two temperature/DO profile stations (42510101 and 42510102) began collecting temperature and DO on 06/12/2023.

Boundary and initial conditions

Heatsource

Heatsource boundary conditions consisted of vegetation and topographic characterization along the length of the river. The primary vegetation characteristics utilised in the model were height and density. Point cloud data were used to create grids of vegetation of height and density, and ground elevation, which were then sampled at regular intervals along the length of the study reach. Vegetation density was estimated by calculating the kernel density of vegetation points throughout the model domain. Vegetation foliage was assumed to be present year-round with no significant or seasonal leaf fall and no change in density.

Tuflow FV

The boundary conditions for the Tuflow FV model included water balance modelling based on inflows and outflows discharge, meteorological forcings (e.g., solar radiation and wind), and mass flux associated with the inflows and outflows. The two study areas presented different opportunities in terms of the hydrology and water quality dynamics.

Inflows and water balance

Culgoa River

SR1 was modelled as an isolated waterhole, not subject to inflows from upstream or outflows at a downstream boundary. System loss was observed through decreasing water levels at a rate greater than what could be accounted for through evaporation, likely due to a combination of loss to groundwater and agricultural abstraction. A time-varying system loss was applied across the whole domain to account for this loss. The rate of variability was used as a calibration parameter to ensure the modelled water level matched the observed water level at the Brenda flow gauge.

Darling River

At SR2, there were three inflow conditions and one outflow condition, all of which were included in the model and estimated using gauged flows from the gauge data available. The two inflows at the upstream boundary of the river, Menindee Main Weir (425997) and Lake Pamamaroo (425995) were combined prior to input to the model domain (Figure 9). Menindee Lake Outlet (425994) discharges into the Darling River in the middle of the model domain downstream of the town of Menindee. The Darling River then discharges out of the model domain at Weir 32 (425012). Flows varied at each station during the period of modelling, with peak flows occurring on 07/01/2024 of 18.3 $m^3 s^{-1}$ (Figure 10). Two other gauges within the domain collect water levels (425034 and 425001; Figure 10) were used in the calibration of the hydrodynamics of the model. Flows from Menindee Main Weir occurred on only a couple of days in the period, whereas flows from Lake Pamamaroo and Menindee Lake comprised the majority of the flow expressed at Weir 32 (425012).

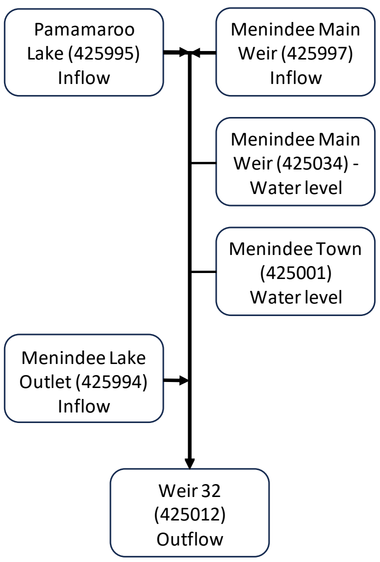

Figure 9. Conceptual model of inflows and outflow of the Darling River at Menindee Lakes.

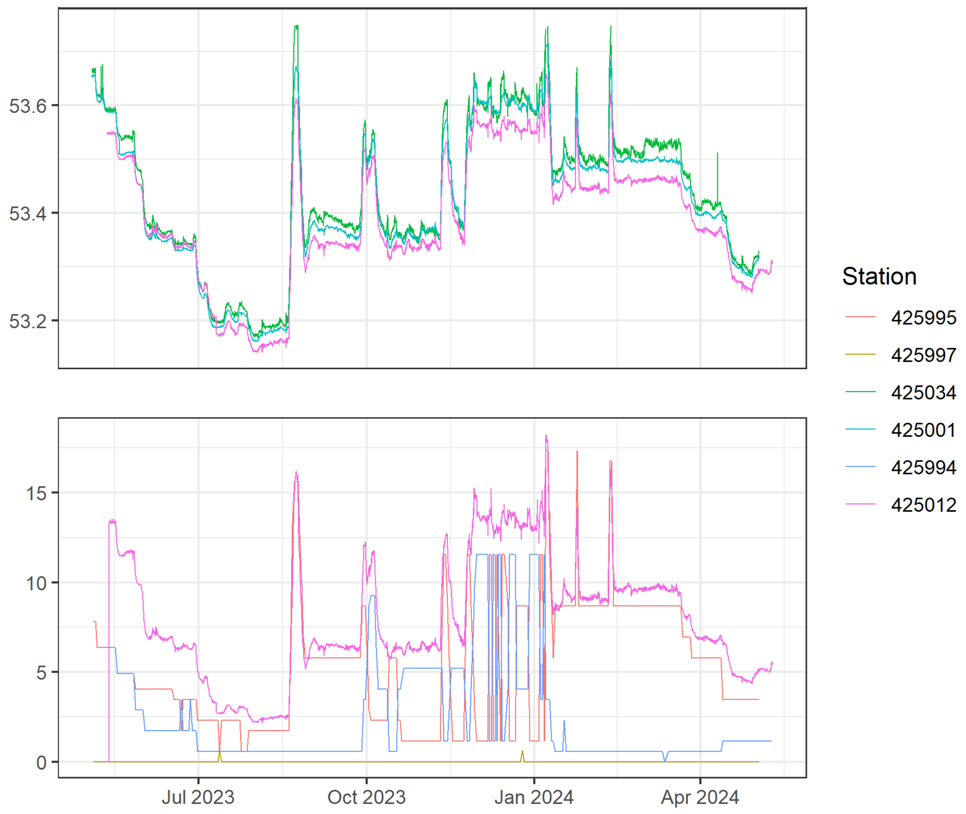

Figure 10. Time series of water level boundary conditions and gauge height for SR2.

Meteorological data and local weather

Shortwave (solar) data

Using the Heatsource-generated dynamic effective shade estimates combined with daily solar radiation measurements from the Mulga Downs BOM station (44054) for SR1, and gridded ERA5[5] for SR2, we generated hourly solar radiation penetrating the vegetation canopy and reaching the ground or water surface. These solar estimates were cast into 50 m x 50 m grids (e.g., Figure 11) covering the entire model domains at hourly time steps throughout modelling periods. In the process of calibrating model thermodynamics at SR1, we reduced the shortwave radiation reaching the surface of the water to simulate light decay in the water column due to high levels of sediment. In some instances, we reduced the solar radiation inputs by as much as 65%.

Wind data

We created 50 m grids from hourly wind measurements at 10 m elevation above the ground were sourced from St. George BOM station (43109) for SR1, and gridded ERA5 for SR2. We applied wind reduction factors (WRF) based on wind reduction subcanopy profiles from Moon et al. (2019). They used measured subcanopy wind profiles of different vegetation categorisations, such as open woodland and scrub/heath, to develop reduction factors as a function of height within the subcanopy. We applied these reduction factors to wind measurements by linking vegetation types within the model domain to one of the Moon et al. (2019) categorisations. The model domain vegetation types were assigned using Regional Ecosystem vegetation mapping for Queensland (Neldner et al., 2022)

---

[5] European Centre for Medium-Range Weather Forecasts (ECMWF) Reanalysis v5 (ERA5) meteorological data. https://www.ecmwf.int/en/forecasts/dataset/ecmwf-reanalysis-v5 using a bounding box of 142.223°E to 142.723°E and 32.623°S to 32.123°S.

and State Vegetation Type Mapping for New South Wales (Roff et al., 2022). The wind boundary conditions were spatially explicit wind estimates broken into hourly grids.

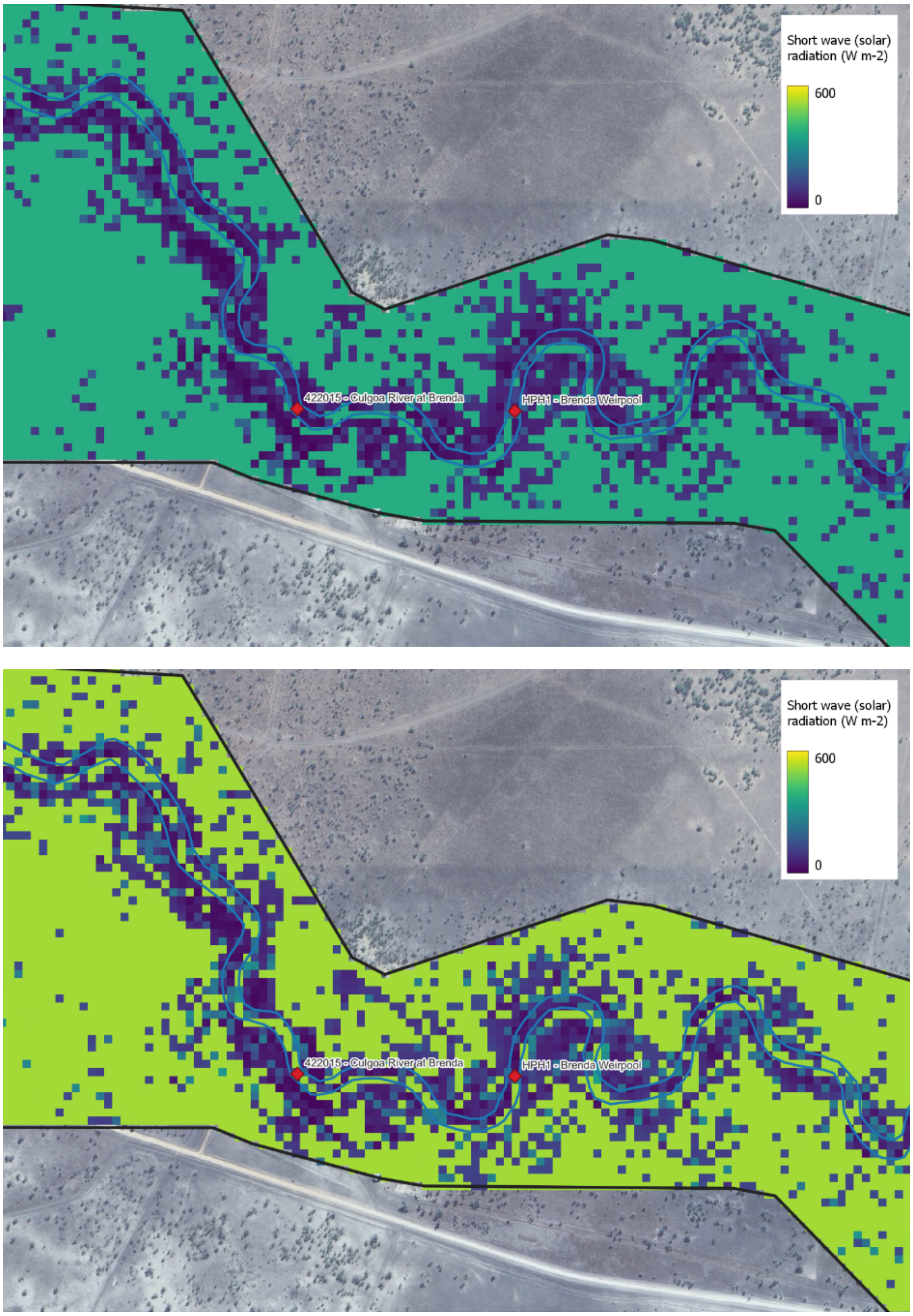

Figure 11. Example of shortwave (solar) radiation reaching the ground and water surface at Brenda waterhole (SR1) based on vegetative and topographic shading at 8 am (top) and 4 pm (bottom) on 15/10/2019. The black line shows the model domain, and the blue lines represent the waterhole delineation from the HPH project.

Air Temperature

Similar to wind and shortwave microclimate adjustments as a result of riparian vegetation, we modified air temperature at the water surface based on vegetation using vegetation density (Klos & Link, 2018). We created 50 m grids of hourly air temperature measurements at 2 m above the ground, sourced from St. George BOM station (43109) for SR1, and gridded ERA5 for SR2.

Other meteorological data

The remainder of the meteorological data were gleaned from the St. George BOM (43109) station as per the HPH project for SR1, and the gridded ERA5 data for SR2 (Figure 12). The data included relative humidity, latent heat, cloud cover and precipitation in hourly observations. Each of these meteorological variables was applied as a global condition (i.e., same value at each model cell).

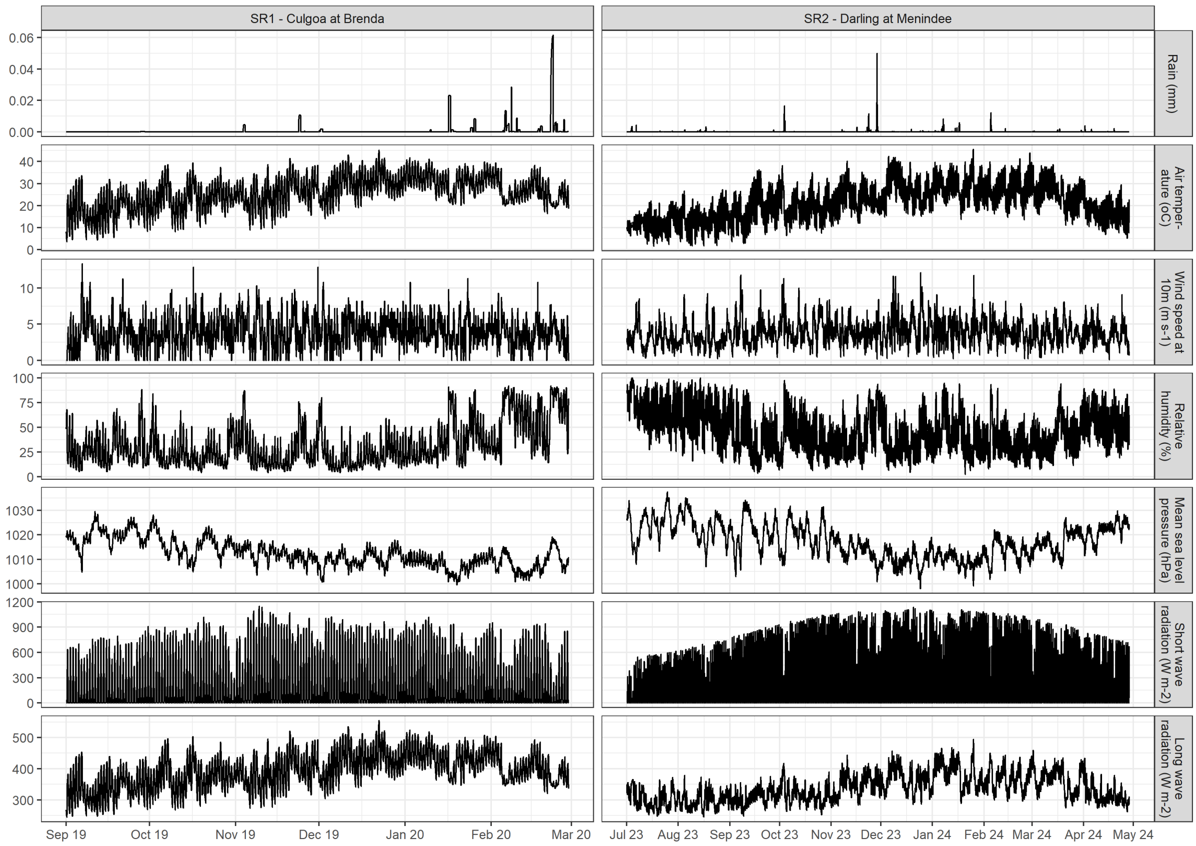

Figure 12. Regional meteorological data for the model inputs representing weather conditions before vegetation modification for microclimate estimates at Culgoa and Darling at Menindee.

Water quality

Culgoa River

For SR1, other water quality data, such as nutrients and phytoplankton biomass were not available during the model time frame. We used data from three additional sources of data as seasonal (monthly) guidelines for output values and model parameters.

The first dataset was quarterly nutrient and physicochemical samples collected by the Queensland government at flow gauges and made available through the Water Monitoring Information Portal (WMIP[6]). Two gauges upstream of the Brenda weir pool were incorporated into the water quality data

[6] https://water-monitoring.information.qld.gov.au

for SR1: 422208B, Culgoa River at Woolerbilla Road and 422204A, Culgoa River at Whyenbah. These data were used in creating initial conditions and calibration guidelines for SR1. The second data set included total nitrogen (TN) total phosphorus (TP), filterable reactive phosphorus (FRP), ammonium (NH_4-N), nitrate (NO_3-N) and suspended sediment concentrations. These data were collected at the Brenda waterhole approximately every quarter from 2007 to 2012 as part of the New South Wales Intersecting Streams surface water plan area (DPIE, 2020). Chlorophyll *a* data include samples collected by the Department of Environment, Science, and Innovation (Hodges, 2018). These data were collected at the Brenda waterhole from August 2017 to April 2018. Samples were collected at the water surface, near the edge of the water and in the benthos. Mean monthly chlorophyll *a* data for the month of September 2017 were used as initial conditions in the model.

These water quality data were used in the setting of initial conditions (Section 0) and providing guidelines for the calibration of the Tuflow FV biogeochemistry (Section 0), but not for boundary inflows because no inflows were modelled for the Brenda waterhole. Given the lack of data to differentiate broad groups of algae, we only modelled one group.

Darling River

For SR2, we used two sets of data to create initial and boundary conditions, as well as provide guide markers for water quality. The first set consisted of WaterNSW sampling data from their API portal[7]. The data collated from this site for this project included TN, TP, turbidity and suspended sediment concentrations. The data available were collected approximately every month during the period of modelling. The second set of data consisted of chlorophyll *a* samples collected by Doyle et al. (2023) in support of the Independent review into the 2023 fish deaths in the Darling-Baaka River at Menindee (Durrant-Whyte, 2023). Chlorophyll *a* samples from this study were collected as a one-off in August 2023. Three sites were sampled by depth and longitudinal profiles (Figure 3).

The water quality data were used to set initial condition (Section 0) and boundary inflow conditions, as well as provide calibration targets (Section 0).

Nutrients

For inflow boundary conditions, water quality data from two sites were used to populate time series inputs, one for the upstream boundary condition at Pamamaroo Lake, and one for Lake Menindee inflow. Both lakes have associated water quality data for creating inflow water quality boundary conditions: Lake Menindee data is located within the lake and Lake Pamamaroo samples are taken at the point of discharge to the Darling River (Figure 13). These data were interpolated at an hourly timestep. Because the water quality data for the Darling River model were presented as total concentrations, we used the values from the Culgoa to develop partitions of total nutrients into speciated constituents, such as ammonium and filterable reactive phosphorus.

Chlorophyll *a*

For chlorophyll *a* data, only data at the upstream most site (S5; Doyle et al., 2023) was available for inflow boundary conditions and was used for both the upstream and Lake Menindee inflow boundary conditions. These data were collected as a one-off rather than the monthly sampling conducted by WaterNSW. Phytoplankton were modelled under one general group, given the lack of data to differentiate broad algal groups.

---

[7] https://api-portal.waternsw.com.au/

Suspended Sediment

No suspended sediment data were available for Lake Pamamaroo or Lake Menindee, but turbidity data were collected during the modelling period. To address this gap, we used a linear relationship between turbidity and suspended sediment from data collected at Weir 32 to develop time series of suspended sediment for the inflow boundary conditions (Figure 13).

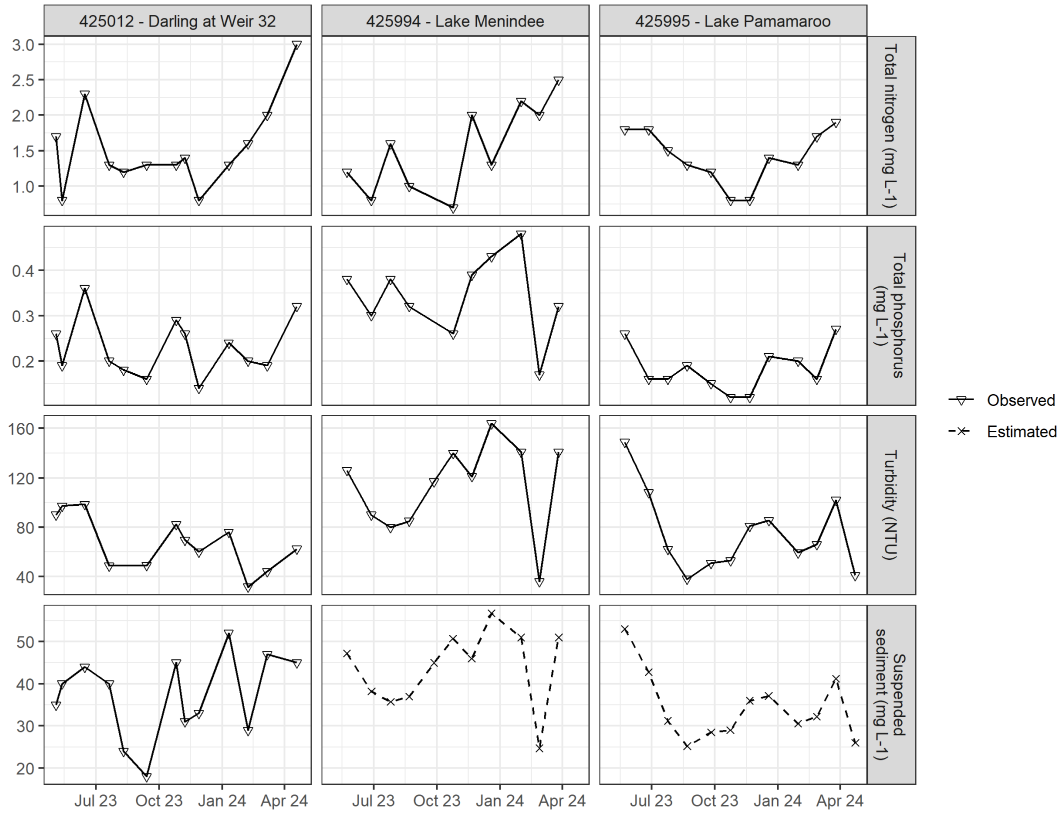

Figure 13. Inflow water quality boundary conditions at Lake Pamamaroo and Lake Menindee. Estimated values of suspended sediment were derived from a linear relationship to turbidity measurements.

Initial conditions

Initial conditions for the two study reaches were based on an amalgamation of sources, typically from previous studies (e.g., HPH) or the state agencies that collected the data (Calibration *evaluation Table 1).*

We used a suite of quantitative and qualitative calibration metrics to assess the performance of the model. We performed all evaluations for the 2D modelled parameters of flow, water level, and for the 3D modelled parameters of temperature and dissolved oxygen. We did not perform calibration for the Heatsource model shade outputs, because we did not have field data for shading or solar input.

These conditions were applied as global values with no stratification. Because initial conditions were specified as depth averaged, we incorporated a model warm-up period of at least 5 days, to allow for st ratification to develop.

Calibration evaluation

We used a suite of quantitative and qualitative calibration metrics to assess the performance of the model. We performed all evaluations for the 2D modelled parameters of flow, water level, and for the 3D modelled parameters of temperature and dissolved oxygen. We did not perform calibration for the Heatsource model shade outputs, because we did not have field data for shading or solar input.

Table 1. Initial water quality conditions for the 3D Tuflow model application.

WQ Variable	Unit	SR1	Source	SR2	Source
Salinity	psu	0.141	WMIP	0.298	WaterNSW
Temperature	°C	11.76	HPH; Zhai et al. (2022)	11.63	WaterNSW
Suspended sediment	mg L^{-1}	75	WMIP	42	WaterNSW
DO	mg L^{-1}	6.39	HPH; Zhai et al. (2022)	9.03	WaterNSW
Silica	mg L^{-1}	15.5	Estimate	20	Estimate
Ammonium	mg N L^{-1}	0.011	WMIP	0.05	WaterNSW
Nitrate-nitrite	mg N L^{-1}	0.15	WMIP	0.314	WaterNSW
Filterable reactive phosphorus	mg P L^{-1}	0.06	WMIP	0.046	WaterNSW
Dissolved organic carbon	mg L^{-1}	2.88	WMIP; Aslam et al. (2013)	2.88	WMIP; Aslam et al. (2013)
Particulate organic carbon	mg L^{-1}	1.73	Petrone et al. (2009)	1.73	Petrone et al. (2009)
Dissolved organic nitrogen	mg L^{-1}	0.094	WMIP	0.231	WaterNSW
Particulate organic nitrogen	mg L^{-1}	0.028	WMIP	0.078	WaterNSW
Dissolved organic phosphorus	mg L^{-1}	0.024	WMIP	0.026	WaterNSW
Particulate organic phosphorus	mg L^{-1}	0.011	WMIP	0.013	WaterNSW
Refractory dissolved organic carbon	mg L^{-1}	1.84	WMIP	1.84	WaterNSW
Refractory dissolved organic nitrogen	mg L^{-1}	0.431	WMIP	1.051	WaterNSW
Refractory dissolved organic phosphorus	mg L^{-1}	0.109	WMIP	0.135	WaterNSW
Refractory particulate organic matter	mg L^{-1}	2.24	WMIP	2.42	WaterNSW
Phytoplankton (chlorophyll *a*)	µg L^{-1}	12.565	Hodges (2018)	33.32	Doyle et al. (2023)

For quantitative metrics, we used the Nash-Sutcliffe efficiency (NSE) and root mean squared error (RMSE) as well as the coefficient of determination (R^2) between the pair-wise comparisons of modelled and observed values. For qualitative comparisons we examined time series plots of modelled and observed values. For the 3D Tuflow model, comparisons were conducted for each depth individually, and for all depths combined. For 2D and 3D Tuflow modelling we also examined scatterplots of pair-wise modelled-observed values. Given the paucity of nutrient, chlorophyll *a*, and sediment data, we only present visual time series comparisons of modelled and observed values. For Culgoa, this can only be done by comparing ranges of values for monthly time periods because the observations and modelling time periods do not overlap. We have used all of the quantitative and qualitative tools in combination to determine the goodness of model fit to the data.

We provide summary statistics of model performance for all model parameters and sites for at each study reach in tabular format within the body of this report. We present representative examples of figures in this report, with the remainder of similar figures in Appendix A. Specifically, for time series plots, we show temperature and DO at the two profile gauges for SR2 (42510101 and 42510102), and for pair-wise scatterplots, we show temperature and DO at the HPH profile station.

Scenarios

We developed scenarios to include climate change, flow management, changes in riparian cover, and combinations of these factors when we have the validated 3D model. Scenarios were conducted under three different general conditions: climate change, riparian vegetation modification, and flow regulation. We believe the assessment of these conditions will provide the Murray Darling Basin Authority valuable information about how to manage key environmental drivers that pose water quality risks to aquatic communities in the basin. While these scenarios do not represent exhaustive implementation possibilities, they encapsulate a range of conditions with practical boundaries from which management can be guided.

We acknowledge the importance of pragmatic constraints on scenario analysis, including the influence of socio-economic factors, and we have developed these scenarios with some consideration of these factors. For example, revegetation and clearing are typically conducted within restoration programs or vegetation management regulation, neither of which we have explicitly sought to simulate. Instead, we have developed scenarios that examine the possible rate of change in both the environmental conditions and the water quality consequences, such as when vegetation is modified by a set amount, how much does available fish habitat change.

The scenario time frames were identical to those for the model calibration, given the limited amount of continuous DO and temperature data available. For the climate scenarios, the modelling time frames were projected into the future under future weather conditions.

Climate Change

We included climate change scenarios (Table 2) to understand the possible impacts of dissolved oxyge n dynamics and risks of hypoxia and anoxia from changing weather patterns.

Our climate change scenarios examine two representative concentration pathways (RCP) and make use of three global climate models (GCM) with CMIP5 initial conditions downscaled using two regional climate models (RCM). We examine the impacts of these changes over the course of the 21st century at 2 intervals of time. (Values *were* applied as percent deviations from conditions during the modelling periods for each project site. For example, if the mean autumn daily maximum temperature (March-April-May) is predicted to rise from 22°C in 2020 to 26°C in 2070 under RCP4.5, an 18% increase was applied to all daily maximum temperature used in the base scenarios for those months. From the combination of seasonal daily mean, minimum and maximum temperatures, hourly time series of temperatures were estimated for each scenario.

These model projections were sourced from the state of New South Wales Climate Data Portal[8]. The variable projections include seasonal (quarterly) values of daily minimum, mean and maximum temperatures, shortwave radiation, wind speed, relative humidity, and long wave radiation.

Values were applied as percent deviations from conditions during the modelling periods for each project site. For example, if the mean autumn daily maximum temperature (March-April-May) is predicted to rise from 22°C in 2020 to 26°C in 2070 under RCP4.5, an 18% increase was applied to all daily maximum temperature used in the base scenarios for those months. From the combination of seasonal daily mean, minimum and maximum temperatures, hourly time series of temperatures were estimated for each scenario.

[8] https://climatedata-beta.environment.nsw.gov.au/

Table 2. Summary of climate change scenario details.

Representation concentration pathway (RCP)	Time intervals	Global climate model (GCM)	Regional climate model (RCM)	Variables included
• RCP4.5 • RPC8.5	• 2020 (base) • 2060 • 2100	NARCliM1.5: • ACCESS1-0 • ACCESS1-3 • CanESM2	• Weather Research and Forecasting (WRF) Model, version 3.6 ○ RM1 ○ RM2	• Minimum, mean, and maximum temperature • Shortwave (solar) radiation • Wind speed • Relative humidity • Long wave (latent) radiation
		These climate projections were averaged for each of the RCPs and time intervals (left columns) and variables (right column)		

For the climate scenarios, all of the inputs and initial conditions were modified to reflect the change in weather. We anticipated that temperature would be a key factor affecting the water column dynamics, including the initial starting temperature of the water and the temperature of the inflow boundary conditions.

Vegetation modification

For vegetation modification scenarios, we simulated changes to riparian vegetation within the model domain to quantify potential benefits or impacts on water quality from that modification. Our scenarios focused on revegetation or removal of vegetation within portions of the near-stream areas. The riparian areas along the length of the reaches within the model domain were divided into subsections and selected at random for clearing or revegetation. We looked at two scenarios for each study reach: (1) revegetation of 70% of the riparian buffers (Olley et al., 2015) and (2) removal of 50 percent of the vegetation within the buffers. These scenarios were developed irrespective of whether vegetation existed within a subsection or not.

Regulation

We conducted two flow scenarios for each study reach, however, unlike the vegetation and climate change scenarios, flow scenarios for each study reach differed based on the differences in the hydrology of the systems.

For SR1, we introduced a flow pulse of approximately two times the volume of the waterhole discharged over the course of a week to estimate the effects of "flushing" the system during a period of no flow. The two scenarios for SR1 considered flushing early in the no flow period (October 2019) and the other considered flushing two months later. The corresponding flow rate for the flushing events was 0.43 $m^3\ s^{-1}$. For the flushing periods we used the waterhole initial conditions as inflow boundary conditions during the period of flushing.

For SR2, we examined the effects of different flow rates on the system. The first scenario looked at very low flows and the second scenario simulated flows at twice the rate observed during the modelling period from each of the inflow boundary conditions. The water quality boundary conditions used for the calibration were used for these scenarios.

Scenario comparisons and analysis

To analyse scenarios, we present and synthesize the outputs of the modelling in several ways to provide different angles from which to consider the results. We present a combination of several visual and quantitative metrics while acknowledging the limitations of these metrics to illustrate the totality of the results and their meaning. The complexity of these models poses challenges in terms of how to evaluate the information they produce; we have attempted to give a comprehensive, practical and succinct assessment as possible.

Within the body of this report, we present a subset of the results in figures and tables. We present results representative of the phenomena occurring or that have significant or surprising implications for water quality and management.

We present the following outputs:

- Curtain profiles. Depth profiles along the length of the model domain (curtains) of mean daily values at depth for temperature and DO for each month of the modelling period. Profile values are given at the water surface, mid water column and at the channel bottom. Monthly values include mean daily minimums, averages, and maximums for the base conditions and deviations from the base conditions for the scenarios.
- Time series. Daily minimum, average and maximum values at the water surface, mid-column and channel bottom for temperature, DO at selected locations. Time series are given at the water surface, mid water column and at the channel bottom.
- Tabular summary of scenario outputs. Combination of the curtain profiles and time series taking mean monthly averages of daily mean values at the key locations selected in the time series plots.
- Water column stability. Schmidt's stability estimated for Brenda waterhole using rLakeAnalyzer (Winslow et al., 2022), and temperature differences (delta T) between the water surface and channel bottom for the Darling River. The two different measures are presented for the different study reaches because SR1 shows similarity to a pond or lake and SR2 is a flowing river for which Schmidt's stability is not typically applied. Schmidt stability is a measure of the amount of energy required to mix the water column fully from top to bottom, and remove any density stratification (e.g., from temperature gradients in the water column).
- Habitat Suitability Index (HSI). Estimates of suitable habitat for three fish species (carp, bony bream, and Golden perch) based on oxygen and temperature tolerance limits proposed by Zhai et al. (2022). Estimates are presented as plots of HSI as a function of depth in the water column at selected locations throughout the modelling period. We also present total suitable habitat within the model domain as a percentage of the total volume of water in the domain throughout the modelling period.

The final piece of information presented is a catalogue of indicator and response variables considered in the modelling, a summary of their values for each study reach, and their correlation to each other for the Base conditions in tabular format. The correlation used is the Spearman's Rank correlation coefficient. We used this statistic because it is non-parametric, and we did not have to make assumptions about the distributions of these variables or the nature of their relationships except monotonicity. Many of the variables could be considered both indicators of conditions as well as responses to other conditions. For example, water temperature is affected by many of the variables within the modelling, such as air temperature, but also impacts DO or habitat suitability. This information is not provided as scenario analysis, because we only present results for the base conditions.

Results

Model development and calibration

Vegetation characteristics

At SR1, vegetation heights ranged between 0 and 15 m and densities of 20 and 100% along the length of the reach, with an increase in height and density toward the upstream end (Figure 14). When locally averaged (i.e., locally estimated scatterplot smoothing – loess), vegetation was between 5 and 10 m tall and 40-60% dense. Right and left bank vegetation are similar with some minor variations. Vegetation at the SR1 monitoring locations represent local maximum for both veg height and density.

At SR2 average vegetation heights were approximately 5 m, with right bank vegetation heights greater toward the downstream and of the reach (Figure 15). Vegetation density followed a similar pattern for SR2, with an average of approximately 35-40%. Right and left bank vegetation were about the same with some minor variations. Overall, there was greater variability in vegetation characteristics in SR2 than SR1 (i.e., greater occurrence of stands of taller vegetation), with similar vegetation heights but lower densities.

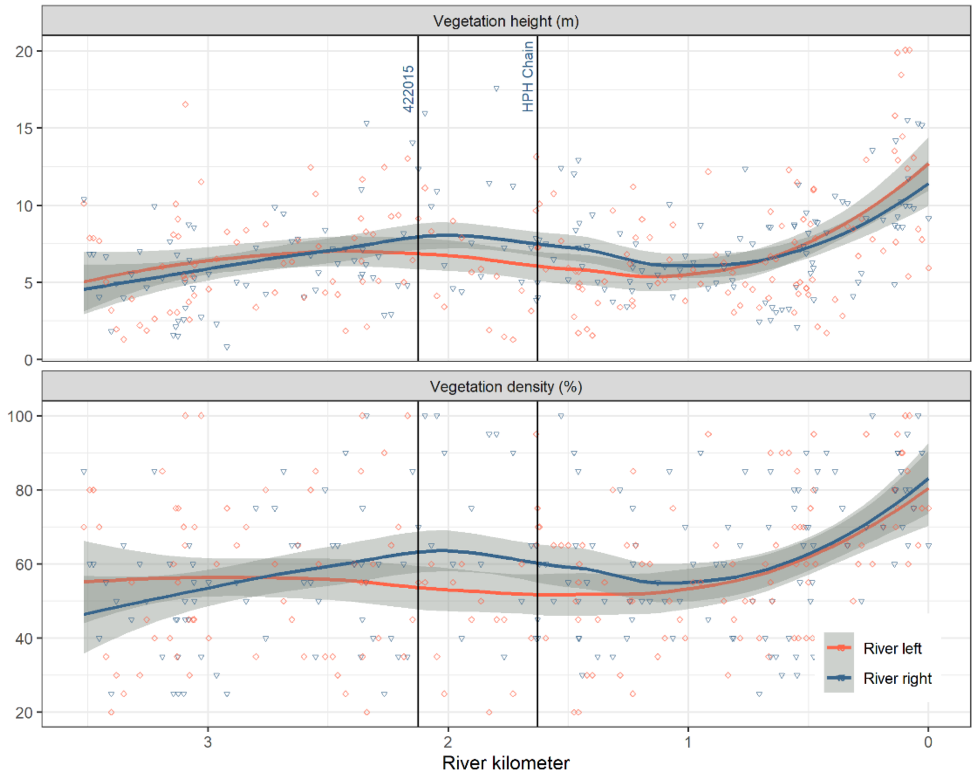

Figure 14. Vegetation height (m) and density (%) from point cloud LiDAR at SR1. Plots show averaged vegetation characteristics along the length of the model domain, with a loess smoothed line and 95% confident intervals. Plots show each side of the river (river right and river left) from the perspective of looking downstream. Landmarks within the domain are provided for reference. Direction of flow (when flowing) is from right to left.

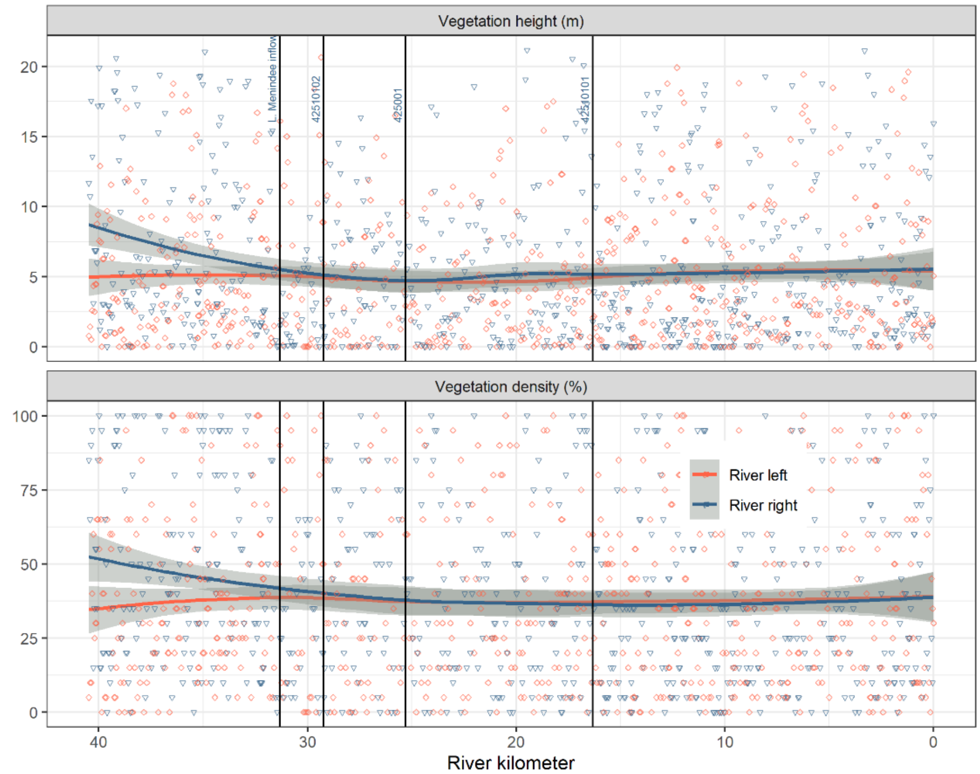

Figure 15. Vegetation height (m) and density (%) from point cloud LiDAR at SR2. Plots show averaged vegetation characteristics along the length of the model domain, with a loess smoothed line and 95% confident intervals. Plots show each side of the river (river right and river left) from the perspective of looking downstream. Landmarks within the domain are provided for reference. Direction of flow (when flowing) is from right to left.

Calibration assessment

Heatsource and shading

The Heatsource model outputs of shortwave radiation allowed us to calculate effective shade at each point within the model domain and use those shade reductions to calculate the solar load reaching the water surface in both space and time.

At SR1, the amount of shortwave radiation reaching the water surface (Figure 16) was consistent with the vegetation patterns observed (Figure 14). That is, taller and more dense vegetation at the upstream and middle portions of the reach resulted in less shortwave radiation at the water surface. At SR2, stands of taller vegetation on the right bank of the Darling River (Figure 15) resulted in less shortwave radiation at the water surface (Figure 17). Shade resulting from the vegetation was generally uniform along the reach of SR2.

At both reaches, shortwave radiation reaching the surface of the water was greatest in the middle of the day (noon), and on the longest day of the year (21 Dec) when the sun is at its highest angle in the sky. Vegetation at SR1 provided greater shading than the vegetation at SR2 at most times of the day, especially as the length of the days increased.

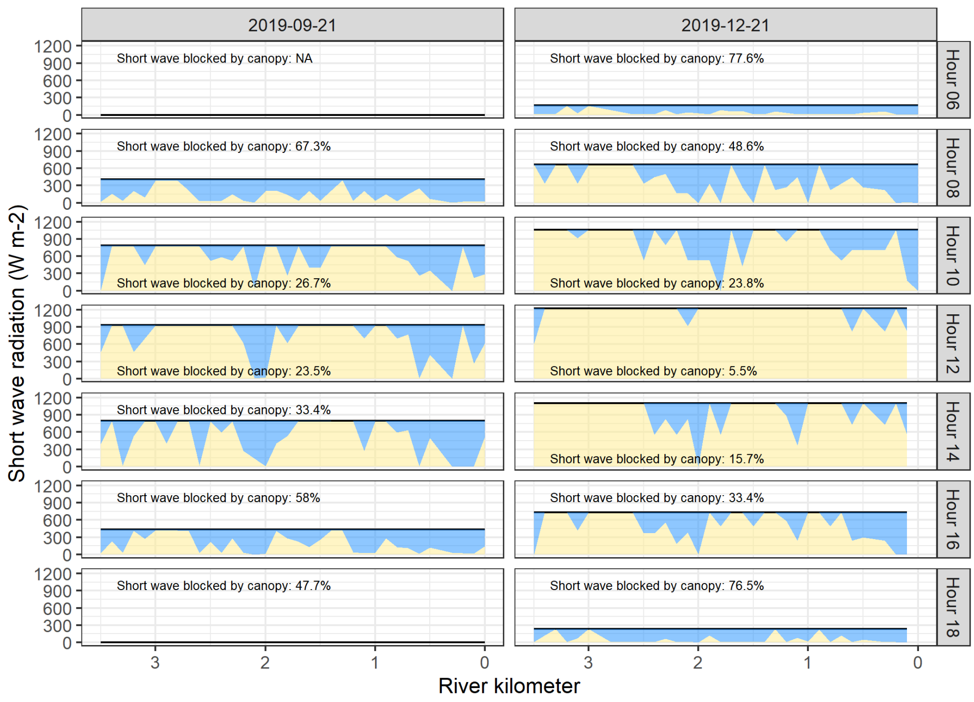

Figure 16. Shortwave radiation at the water surface (yellow ribbon) and total incoming shortwave radiation above the canopy (combined yellow and blue) at SR1 throughout the days of 21/09/2019 and 21/21/2019. Direction of flow (when flowing) is from right to left.

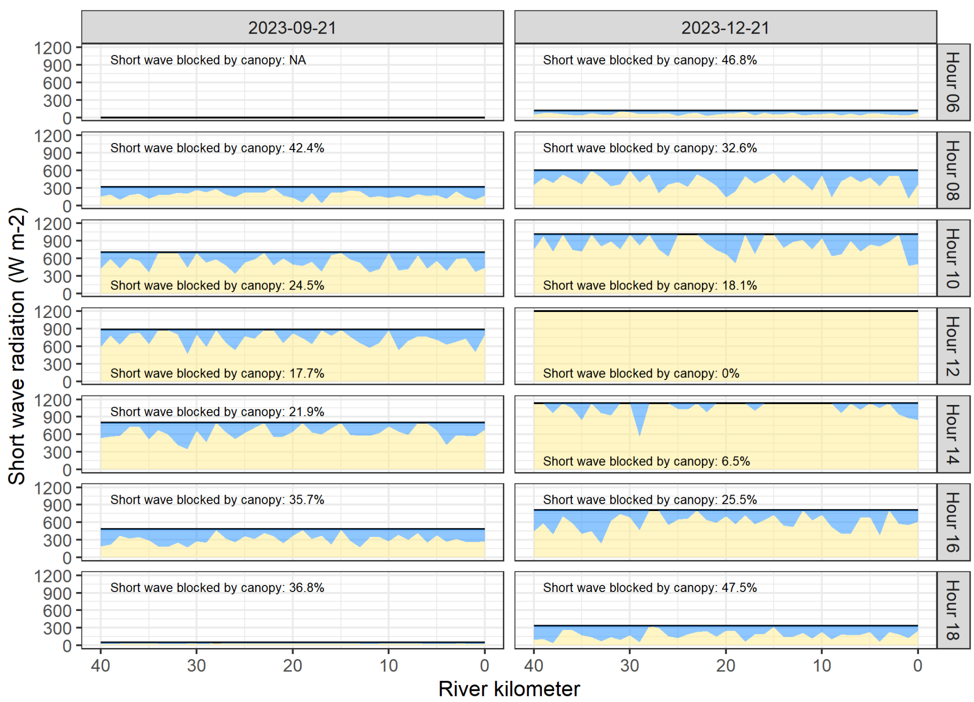

Figure 17. Shortwave radiation at the water surface (yellow ribbon) and total incoming shortwave radiation above the canopy (combined yellow and blue) at SR2 throughout the days of 21/09/2023 and 21/21/2023. Direction of flow (when flowing) is from right to left.

Tuflow FV

The Tuflow FV model was able to simulate both thermodynamics and oxygen dynamics adequately throughout the season for both study reaches, particularly in the deeper parts of the channel. In general, the model captured fluctuations related to changing weather and inflow patterns.

For SR1, the model replicated decreasing oxygen in the water column and during the modelling period (Figure 18 and Table 3). The waterhole became hypoxic near and at the surface eventually becoming anoxic in February, however, the model only captured some hypoxic conditions, particularly at the hypolimnion (near the bottom of the water column). Toward the end of the modelling period observed DO concentrations in the epilimnion (near the surface of the water) had a larger diurnal (day-night) range, which the model captured to some degree. Modelled DO concentrations explained approximately half of the variance in the observed DO concentrations, with errors for all depths at 1.7 mg L^{-1}. Temperatures were predicted well by the model with diurnal and seasonal dynamics replicated well through the modelling period and at all depths (Figure 19 and Table 3). Modelled temperatures were well correlated with observed temperature and explained most of the variance of the observations ($R^2 > 0.9$).

For SR2, the model captured seasonal dynamics of DO based on the time series (Figure 20 and Figure 21) at 42510101 and 42510102, particularly deeper in the water column. For those stations, the model generally predicted smaller diurnal changes in DO at the surface than what are observed, and it slightly underpredicted mean daily DO concentrations. The error (RMSE) of DO predictions for 42510101 and 42510102 was slightly higher for SR1 (Table 4; RMSE = 1.9-2.2 mg L^{-1}) than for SR1. Modelled DO concentrations at 425012 (Weir 32; Table 4) demonstrated a higher correlation to observations than the stations with the profiles.

Like SR1, the model predicted temperature at SR2 very well, capturing seasonal and diurnal dynamics accurately at all stations (Table 4). We have provided time series plots of nutrients and sediment simulated for SR2 by the model (Figure 22), but not calibration performance metrics given the small sample size of observations. We have relied on visual evaluation of the model performance for nutrients and believe that it captured nutrient biogeochemistry adequately. Nutrient data could not be sourced for SR1 during the modelling period but comparisons were made between the ranges of values modelled to ranges of observations (see Appendix A). Hydrodynamic calibration for both study reaches was good, with NSE and R^2 greater than 0.90 (Table 3 and Table 4).

The scatterplots of pairwise model and observed DO and temperature (Figure 23 and Figure 24) show similar model performance as demonstrated in the time series plots and summary of performance tables. At the surface the model slightly overpredicted DO concentrations at higher and lower observed DO values, while underpredicting DO concentrations in the mid-range of observed values. The best relationships were at depths of 1.25 and 1.75 m.

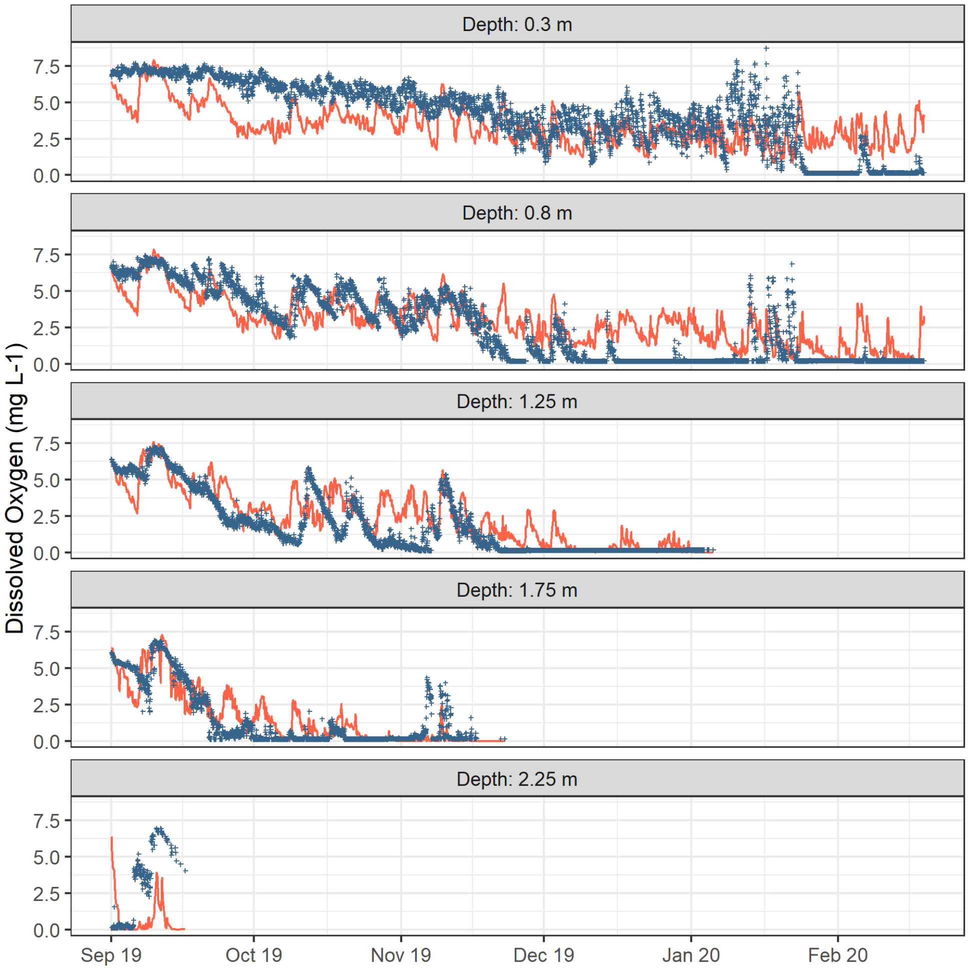

Figure 18. Time series comparisons of observed (blue points) and modelled (red line) DO concentrations at the depths recorded for SR1 during the HPH project during the calibration time frame.

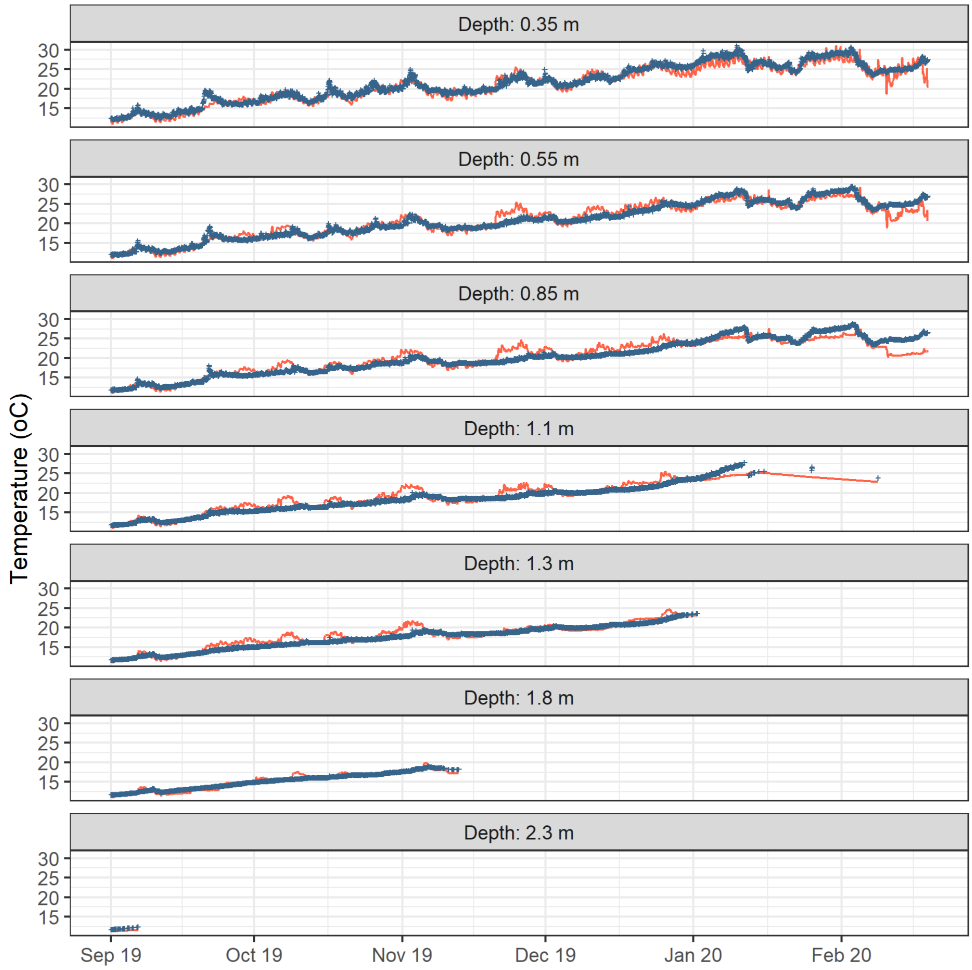

Figure 19. Time series comparisons of observed (blue points) and modelled (red line) water temperatures at the depths recorded for SR1 during the HPH project during the calibration time frame.

Table 3. Tuflow FV 3D model performance for SR1 for dissolved oxygen at each measured depth, and for all depth combined (All depths). RMSE units are specific to each variable (temperature, DO).

Station	Parameter	Depth (m)	*n*	NSE	RMSE	R^2
422015	Water level (m)	-	4105	0.97	0.08	0.99
422015	Temperature (°C)	-	2118	0.54	3.19	0.76
HPH Chain	Dissolved oxygen (mg L^{-1})	0.3	4104	0.24	1.97	0.35
		0.8	4105	0.50	1.65	0.55
		1.25	2995	0.51	1.44	0.62
		1.75	1813	0.66	1.22	0.68
		2.25	244	-0.85	3.31	0.00
		All depths	**13261**	**0.51**	**1.71**	**0.51**
HPH Chain	Temperature (°C)	0.35	4105	0.93	1.22	0.94
		0.55	4105	0.92	1.30	0.92
		0.85	4105	0.87	1.59	0.87
		1.1	3194	0.87	1.26	0.89
		1.3	2896	0.86	1.12	0.89
		1.8	1681	0.92	0.56	0.94
		2.3	67	-5.98	0.46	0.01
		All depths	**20153**	**0.92**	**1.27**	**0.92**

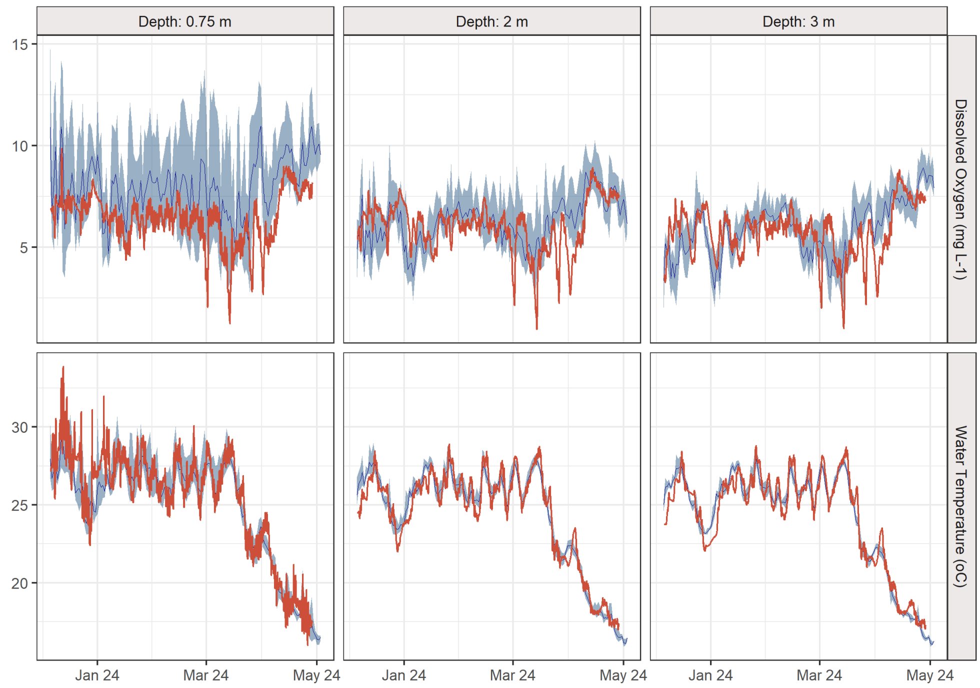

Figure 20. Time series comparisons of observed DO daily range (blue ribbon) and mean daily DO (blue line) and modelled (red line) DO concentrations (top row) and water temperatures (bottom row) at recorded depths at 42510101 for SR2 during the calibration time frame.

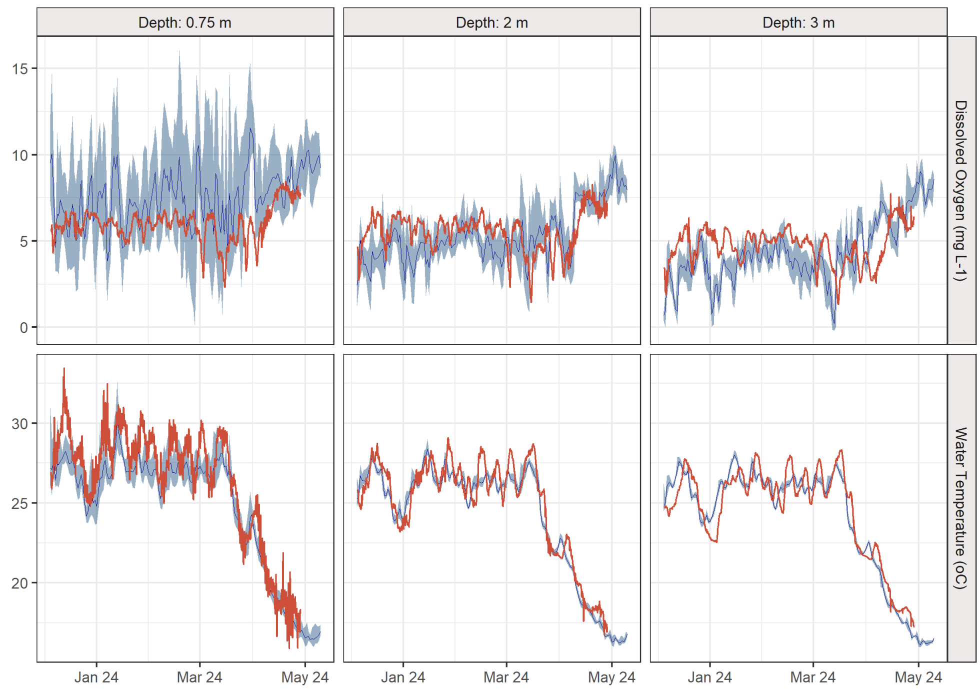

Figure 21. Time series comparisons of observed DO daily range (blue ribbon) and mean daily DO (blue line) and modelled (red line) DO concentrations (top row) and water temperatures (bottom row) at recorded depths at 42510102 for SR2 during the calibration time frame.

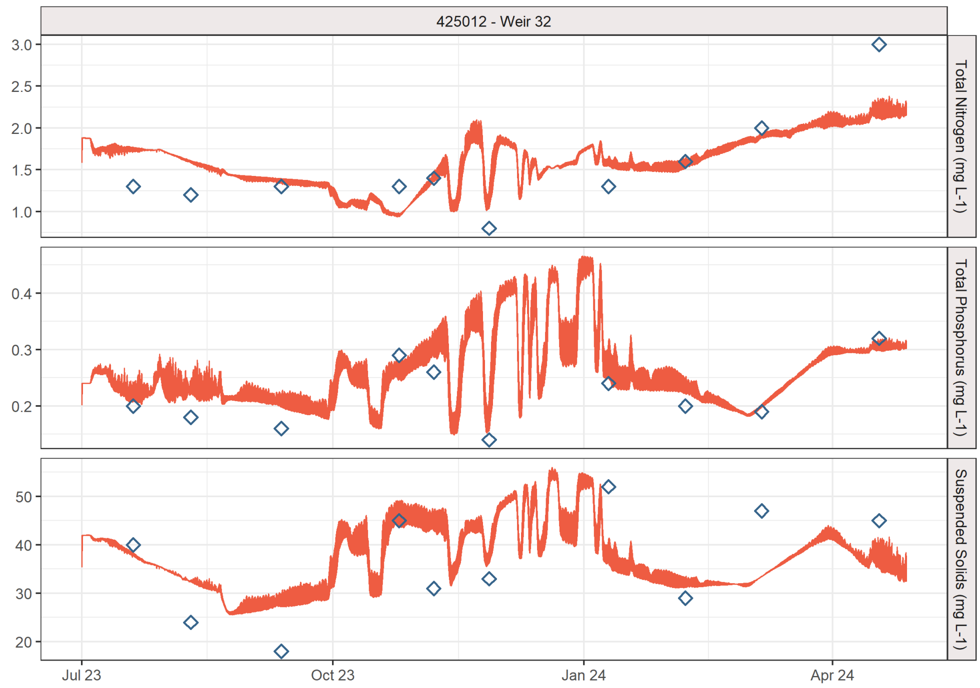

Figure 22. Time series comparison of observed (blue points) and modelled (red line) nitrogen (top), phosphorus (middle) and sediment (bottom) concentrations sampled at 425012 for SR2 during the calibration time frame.

Table 4. Tuflow FV 3D model performance for SR2 for temperature at each measured depth, and all depths combined (All depths). RMSE units are specific to each variable (temperature, flow, water level, DO).

Station	Parameter	Depth (m)	*n*	NSE	RMSE	R^2
425001	Water level (m)	-	7236	0.57	0.09	0.97
425001	Temperature (°C)	-	7235	0.91	1.57	0.97
425012	Dissolved oxygen (mg L^{-1})	-	7239	0.20	2.01	0.46
425012	Flow (m^3 s^{-1})	-	7249	0.92	0.98	0.93
425012	Temperature (°C)	-	7239	0.95	1.18	0.98
42510101	Dissolved oxygen (mg L^{-1})	0.75	3447	-0.65	2.64	0.04
		2	3447	-0.18	1.39	0.16
		3	3448	-0.01	1.35	0.21
		All depths	**10342**	**-0.06**	**1.89**	**0.14**
42510101	Temperature (°C)	0.75	3445	0.77	1.58	0.80
		2	3448	0.94	0.76	0.94
		3	3450	0.94	0.75	0.94
		All depths	**10343**	**0.88**	**1.10**	**0.88**
42510102	Dissolved oxygen (mg L^{-1})	0.75	3470	-0.41	2.94	0.01
		2	3471	-0.24	1.65	0.08
		3	3471	-0.33	1.86	0.04
		All depths	**10412**	**0.11**	**2.22**	**0.13**
42510102	Temperature (°C)	0.75	3469	0.74	1.64	0.88
		2	3469	0.91	0.91	0.92
		3	3472	0.89	0.96	0.90
		All depths	**10410**	**0.85**	**1.22**	**0.88**

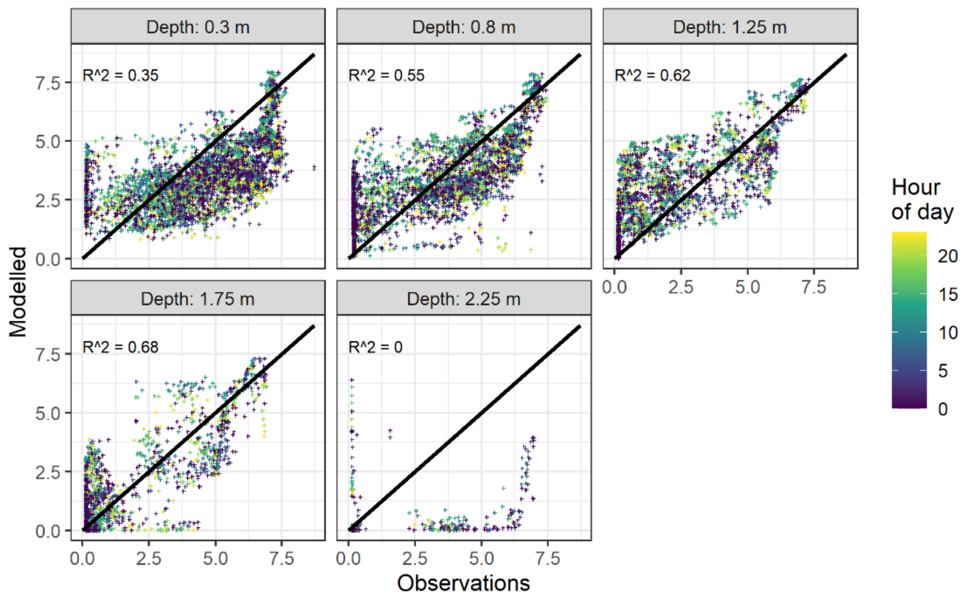

Figure 23. Pair wise observation-model scatterplots of DO concentrations (mg L^{-1}) at recorded depths from the HPH chain at SR1 during the calibration period. The colour gradient refers to the hour of day the observation-model pair occurred.

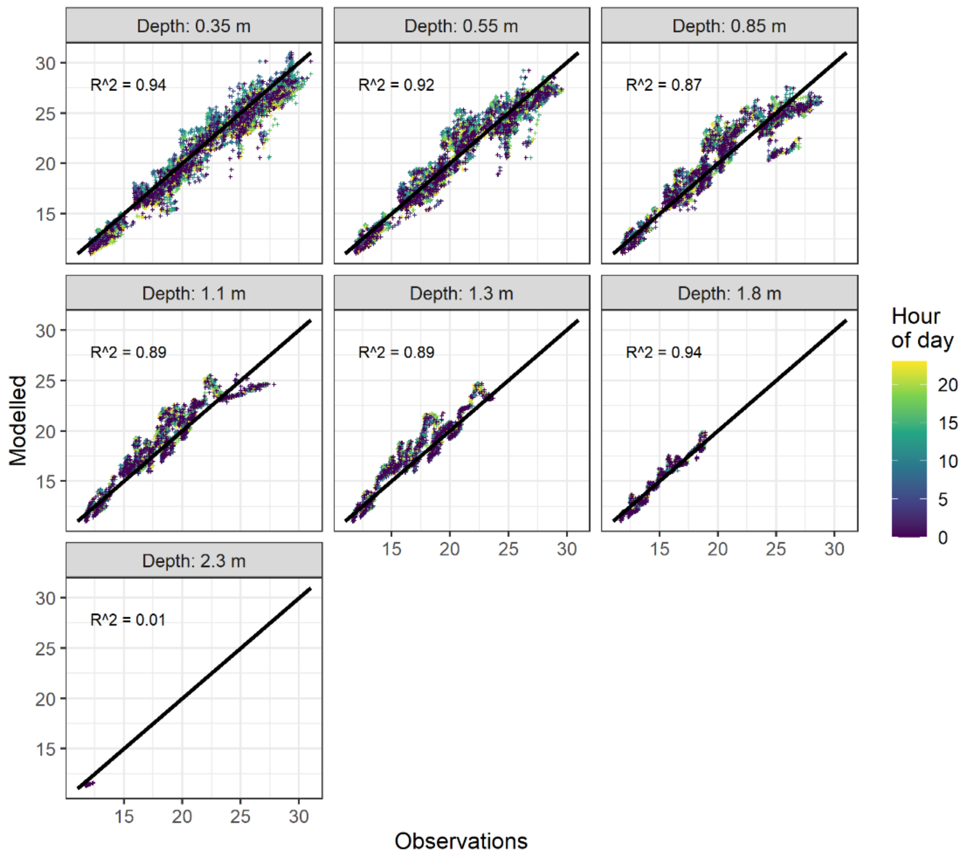

Figure 24. Pair wise observation-model scatterplots of water temperature (°C) at recorded depths from the HPH chain at SR1 during the calibration period. The colour gradient refers to the hour of day the observation-model pair occurred.

Tuflow FV model parameters

Based on the calibration evaluation, we present in this section a subset of key Tuflow FV parameters (*Table 5*). The entire set of parameters is given in Appendix B. The model was first calibrated for the Culgoa River at the Brenda weir pool, and those parameters were ported to the Darling River at Menindee Lakes, with modification to suit the calibration of that study area.

Table 5. Key Tuflow model parameters, units and ranges used.

Group	Parameter	Units	SR1	SR2
Benthic flux parameters	Sediment oxygen demand (SOD)	mg O_2 m^{-2} d^{-1}	-5000	-1000
	SOD half saturation concentration	mg O_2 L^{-1}	0.80	4.80
	SOD temperature coefficient	-	1.10	1.10
Inorganic nitrogen	Nitrification rate	d^{-1}	1.00	1.00
	Nitrification half saturation concentration	mg O_2 L^{-1}	4.80	4.80
	Nitrification temperature coefficient	-	1.10	1.10
	Denitrification rate	d^{-1}	0.23	0.23
	Denitrification half saturation concentration	mg O_2 L^{-1}	0.89	0.89
	Denitrification temperature coefficient	-	1.03	1.03
Organics	Organic carbon hydrolysis rate	d^{-1}	0.10	0.10
	Organic matter mineralisation rate	d^{-1}	0.02	0.02
Phyto-plankton	Growth rate	d^{-1}	1.00	3.50
	Growth rate temperature coefficient	-	1.04	1.10
	Respiration rate	d^{-1}	0.01	0.00
	Respiration rate temperature coefficient	-	1.05	1.04
	Fraction of respiration that is true respiration	-	0.08	0.08
	Carbon to chlorophyll *a* mass ratio	-	30.0	30.0
	Nitrogen to chlorophyll *a* mass ratio	-	4.76	4.76
	Int. phosphorus to chlorophyll *a* mass ratio	-	0.60	0.60

Scenarios

Scenario results are presented in the following subsections in a variety of ways. We have truncated the names of the scenarios in the figures, tables and text for ease of display (Table 6).

Table 6. Scenario names and description summary for each study reach and scenario group.

Abbreviation	Description SR1 - Culgoa	Description SR2 - Darling
Base	Existing conditions - present-day with no modifications	
Climate 1	Climate change - RCP 4.5 year 2060	
Climate 2	Climate change - RCP 4.5 year 2100	
Climate 3	Climate change - RCP 8.5 year 2060	
Climate 4	Climate change - RCP 8.5 year 2100	
Vegetation 1	Vegetation modification - 70% revegetation	
Vegetation 2	Vegetation modification - 50% clearing	
Flow 1	October Flushing	Low flow
Flow 2	December Flushing	Twice the flow as base

Curtain profiles

In this section we provide examples of mean daily simulated DO concentrations and temperature in the water column as a function of distance along the reach for base conditions. We show how different scenarios with varying forcing conditions differ from a base case.

Base DO concentrations for SR1 (Figure 25) showed DO stratification with higher concentrations near the surface of the water for January, and greater stratification occurring when the daily maximum values occur. Compared to climate scenario 4, which shows global decreases in DO concentrations, the greatest decrease in DO occurred at the surface for daily minimum, mean and maximum values (Figure 26), with daily maximum DO values most impacted. Overall, the climate scenarios gave predicted decreases in DO at SR1 by 10 to 32% for January at selected locations. Under 70% increase in vegetation, DO concentrations were predicted to remain about the same (Figure 27), with slight decreases at some locations toward the lower end of the reach. Vegetation scenario 2 showed DO increases of up to 1 to 2 mg L^{-1} at some of the selected sites. For flow scenario 1, daily minimum DO concentrations in January increased up to 1.0 mg L^{-1} at the surface (Figure 28), while daily maximum DO concentrations in that month decreased by as much as 1.0 mg L^{-1} toward the hypolimnion. In general, daily mean DO concentrations for all of the climate scenarios decreased, with climate scenario 4 demonstrating the greatest decrease in DO at all depths and locations (Table 7). Daily temperatures were mostly predicted to increase under all climate scenarios, while temperatures for the flow and vegetation scenarios were approximately the same as base conditions.

Daily water temperatures for the base condition at SR2 (Figure 29 and Table 10) were approximately 30 °C at the top of the water column in January. For most other times in warmer months, water temperatures were generally 25-30 °C. The average increase in temperatures under climate scenario 2 were less than 2 °C, except for daily maximum temperatures in the upper regions of the reach, where some increases were >2°C (Figure 30 & Table 10). Vegetation scenario 2 showed that daily temperatures could increase slightly, particularly when the water was warmest (Figure 31 & Table 10). Flow scenario 2 demonstrated that temperatures could decrease at the surface for any given time of day, while increasing deeper in the water column (Figure 32 & Table 10). DO concentrations were predicted to decrease globally under the climate change scenarios and flow scenario 1 (Table 9).

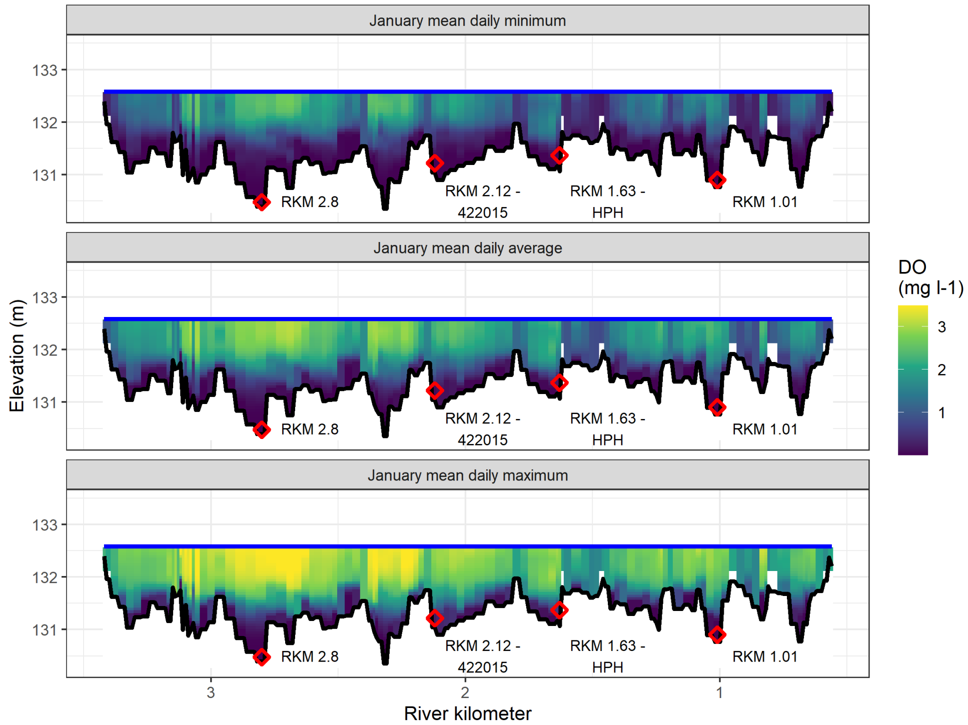

Figure 25. Longitudinal curtain (distance and depth) of dissolved oxygen (DO) concentrations for SR1 for the month of January for base conditions. Panels represent mean daily minimum (top), mean daily average (middle), and mean daily maximum (bottom) concentrations, with cardinal locations provided (red diamonds). Upstream corresponds to the rights side of the figure and downstream to the left. RKM refers to river kilometre.

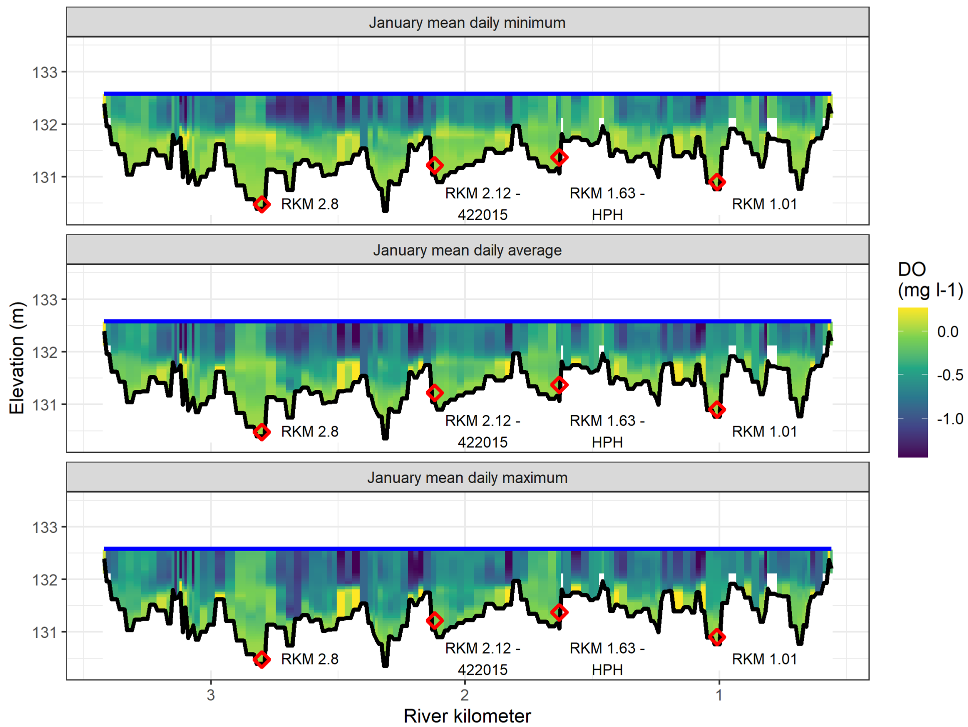

Figure 26. Longitudinal curtain (distance and depth) of the deviation of Climate 4 dissolved oxygen (DO) concentrations from base DO concentrations for SR1 for the month of January. Panels represent mean daily minimum (top), mean daily average (middle), and mean daily maximum (bottom) concentrations, with selected locations provided (red diamonds). Upstream corresponds to the rights side of the figure and downstream to the left. RKM refers to river kilometer.

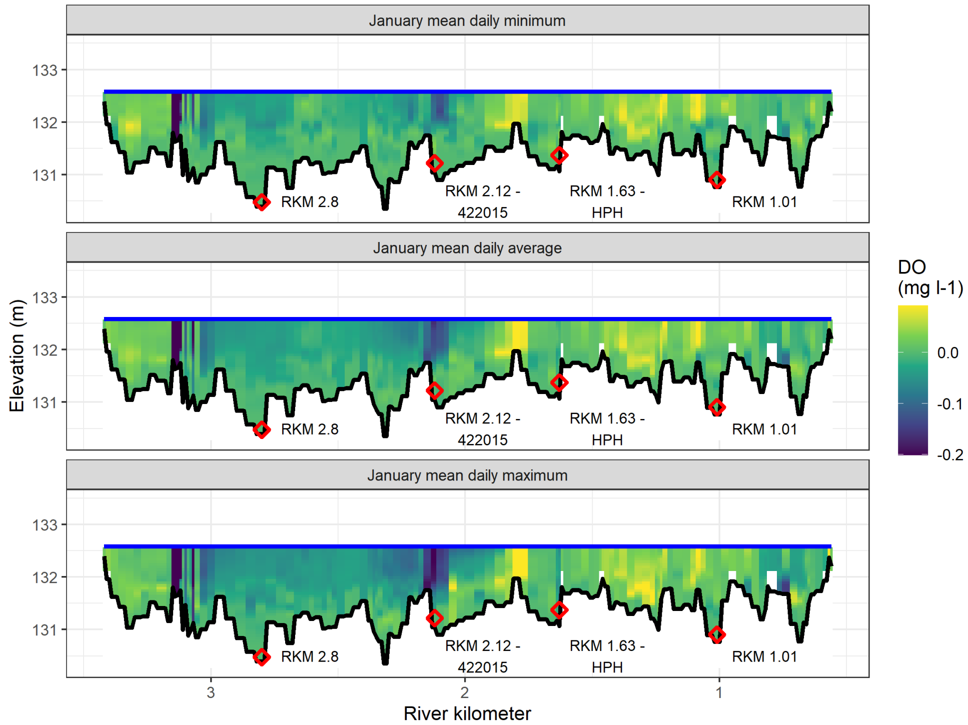

Figure 27. Longitudinal curtain (distance and depth) of the deviation of Vegetation 1 DO concentrations from base DO concentrations for SR1 for the month of January. Panels represent mean daily minimum (top), mean daily average (middle), and mean daily maximum (bottom) concentrations, with cardinal locations provided (red diamonds). Upstream corresponds to the rights side of the figure and downstream to the left. RKM refers to river kilometer.

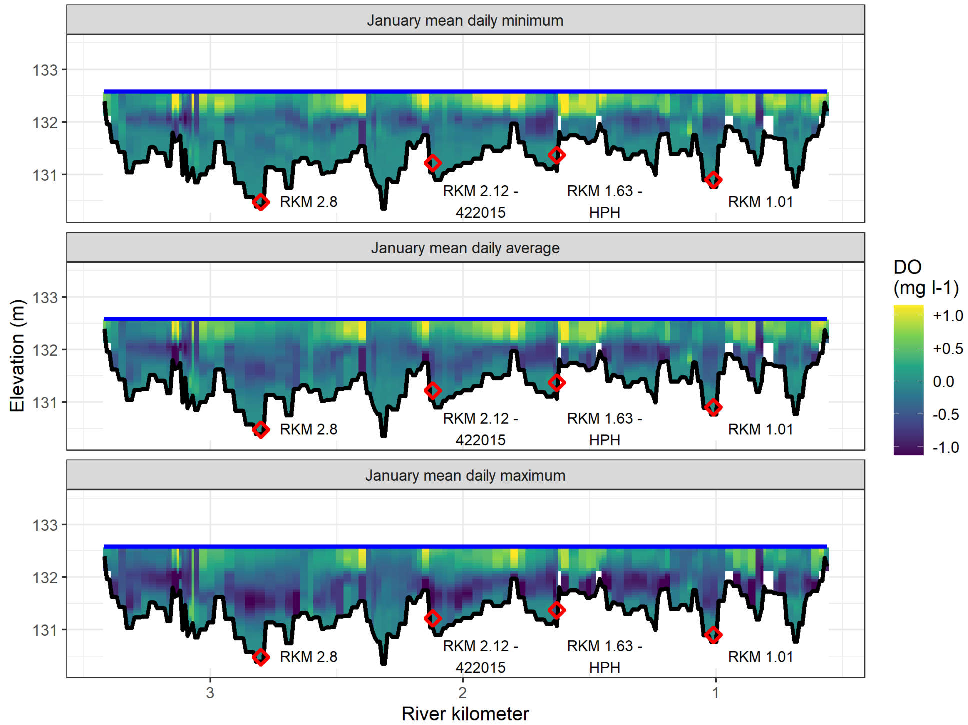

Figure 28. Longitudinal curtain (distance and depth) of the deviation of Flow 1 DO concentrations from base DO concentrations for SR1 for the month of January. Panels represent mean daily minimum (top), mean daily average (middle), and mean daily maximum (bottom) concentrations, with cardinal locations provided (red diamonds). Upstream corresponds to the rights side of the figure and downstream to the left. RKM refers to river kilometer.

Table 7. Daily mean DO concentrations in the water column at SR1 for the month of January for all scenarios at selected locations. Red coloured text for scenarios indicates DO concentrations that are less than the base conditions, and blue coloured text indicates concentrations that are greater than the base conditions. Note this table does not include daily minimum or maximum DO concentrations. Rkm is river kilometer.

Location	Depth	Base	Climate				Flow		Vegetation	
			1	2	3	4	1	2	1	2
Rkm 1.01	Surface	2.14	1.81	1.83	1.79	1.50	2.20	2.03	2.16	4.28
	Mid	1.39	1.27	1.33	1.28	1.09	0.96	0.86	1.42	3.57
	Bottom	0.00	0.00	0.00	0.00	0.00	0.00	0.00	0.00	0.00
Rkm 1.63 HPH chain	Surface	2.19	1.99	1.99	1.97	1.72	2.22	2.01	2.17	2.22
	Mid	1.54	1.48	1.55	1.49	1.26	1.08	1.04	1.51	1.77
	Bottom	0.00	0.00	0.00	0.00	0.00	0.00	0.00	0.00	0.00
Rkm 2.12 422015	Surface	2.24	1.93	1.93	1.91	1.54	2.74	2.53	2.08	3.66
	Mid	1.72	1.50	1.52	1.50	1.14	1.14	1.02	1.60	3.41
	Bottom	0.06	0.06	0.07	0.06	0.02	0.02	0.01	0.06	0.62
Rkm 2.80	Surface	2.92	2.80	2.84	2.81	2.58	3.17	2.93	2.88	3.65
	Mid	1.39	1.33	1.37	1.33	1.27	0.68	0.55	1.37	2.70
	Bottom	0.00	0.00	0.00	0.00	0.00	0.00	0.00	0.00	0.00

Table 8. Daily mean temperatures in the water column at SR1 for the month of January for all scenarios at selected locations. Red coloured text for scenarios indicates water temperatures that are greater than the base conditions, and blue coloured text indicates water temperatures that are less than the base conditions. Note this table does not include daily minimum or maximum temperatures. Rkm is river kilometer.

Location	Depth	Base	Climate				Flow		Vegetation	
			1	2	3	4	1	2	1	2
Rkm 1.01	Surface	26.6	28.2	28.0	28.1	31.4	26.1	26.1	26.6	25.3
	Mid	25.5	27.1	26.9	27.0	30.1	25.3	25.4	25.6	24.8
	Bottom	18.0	19.2	19.3	19.2	21.0	17.3	18.5	18.1	18.1
Rkm 1.63 HPH chain	Surface	26.0	27.7	27.6	27.6	31.0	26.1	26.1	26.0	26.2
	Mid	25.3	27.1	26.9	27.0	30.3	25.5	25.6	25.4	25.6
	Bottom	17.9	19.4	19.5	19.4	21.9	16.4	17.4	18.1	18.2
Rkm 2.12 422015	Surface	26.1	27.8	27.6	27.7	31.0	25.8	25.8	26.3	25.5
	Mid	25.6	27.4	27.3	27.3	30.7	25.2	25.3	25.9	25.4
	Bottom	24.6	26.3	26.3	26.3	29.4	24.1	24.5	24.8	24.8
Rkm 2.80	Surface	26.6	28.3	28.2	28.2	31.7	26.3	26.2	26.8	26.3
	Mid	25.3	26.9	26.8	26.8	30.2	24.5	24.5	25.4	25.6
	Bottom	19.2	20.2	20.4	20.3	22.0	19.1	18.7	19.2	20.6

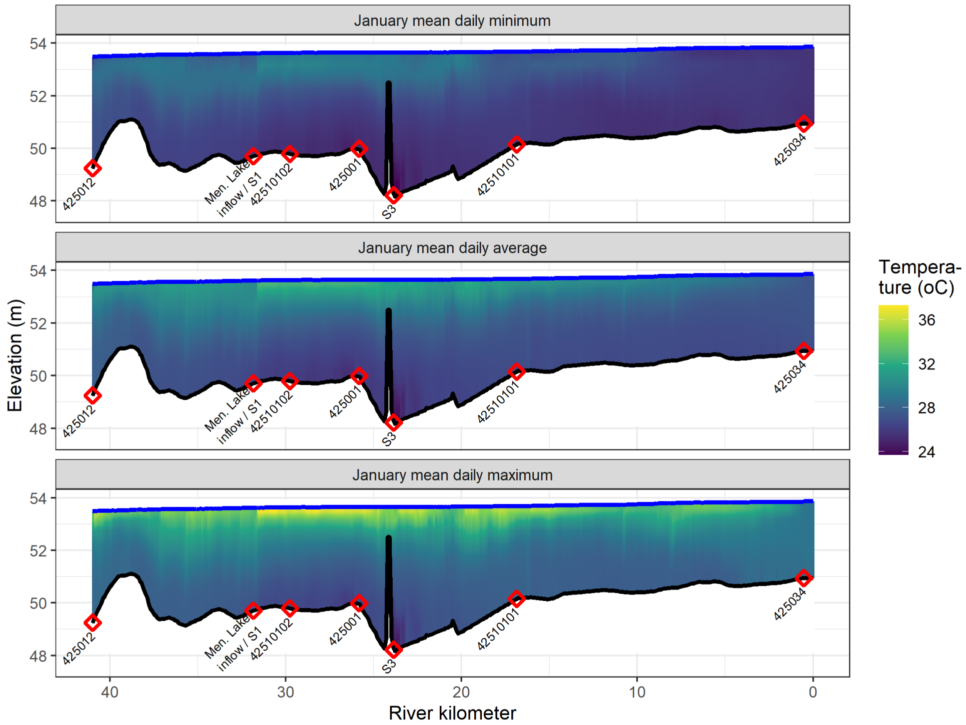

Figure 29. Longitudinal curtain (distance and depth) of water temperatures for SR2 for the month of January for base conditions. Panels represent mean daily minimum (top), mean daily average (middle), and mean daily maximum (bottom) concentrations, with cardinal locations provided (red diamonds). Upstream corresponds to the rights side of the figure and downstream to the left. Rkm refers to river kilometer.

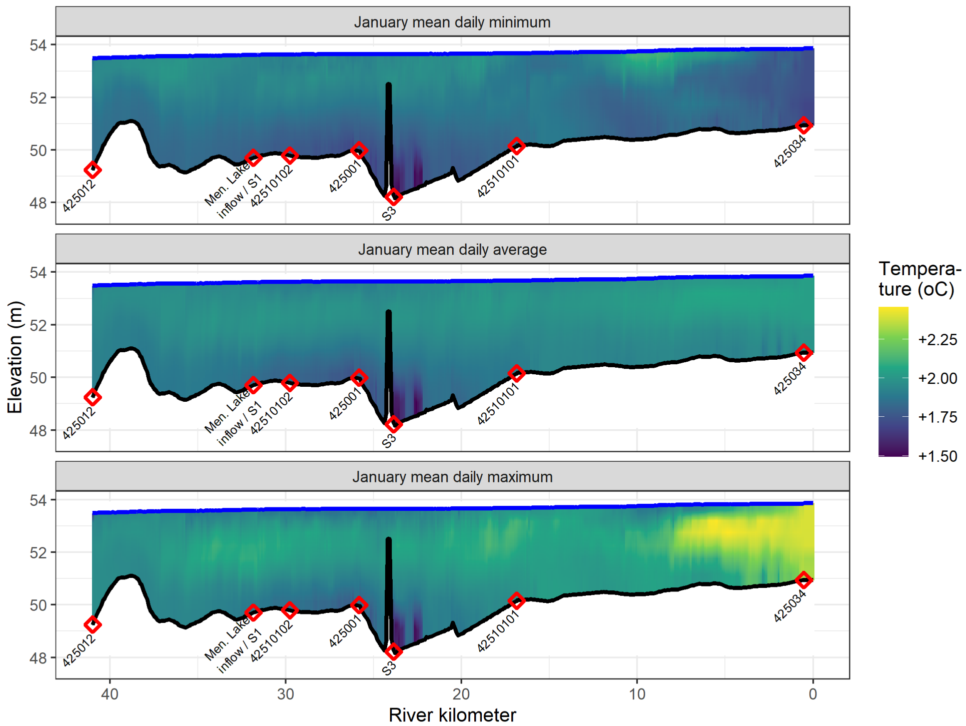

Figure 30. Longitudinal curtain (distance and depth) of the deviation of Climate 2 water temperatures from base water temperatures for SR2 for the month of January. Panels represent mean daily minimum (top), mean daily average (middle), and mean daily maximum (bottom) concentrations, with cardinal locations provided (red diamonds). Upstream corresponds to the rights side of the figure and downstream to the left. Rkm refers to river kilometer.

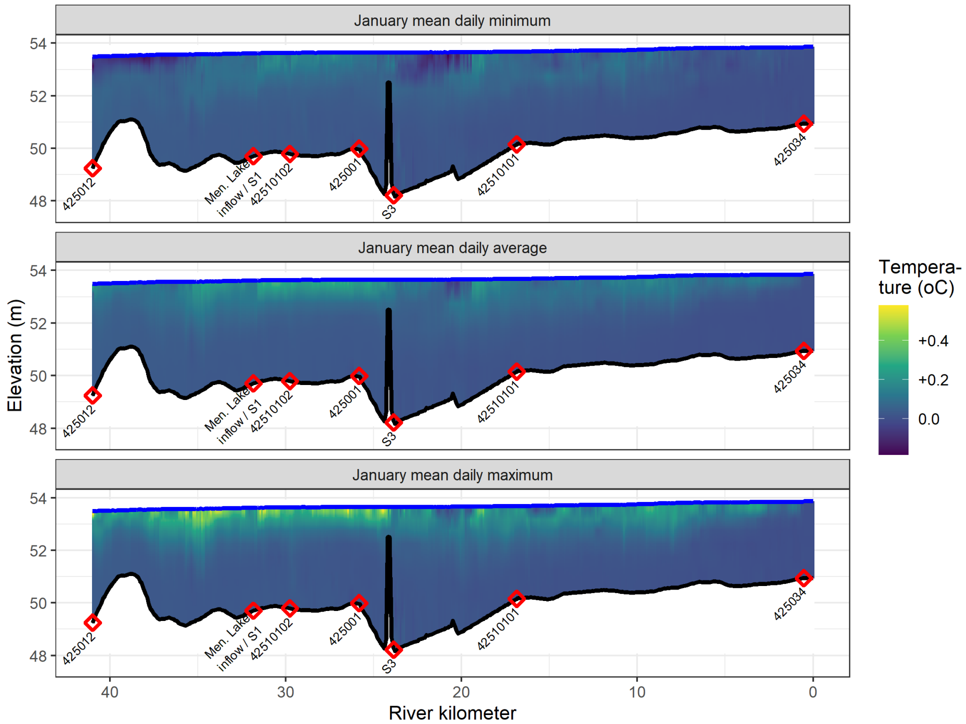

Figure 31. Longitudinal curtain (distance and depth) of the deviation of Vegetation 2 water temperatures from base water temperatures for SR2 for the month of January. Panels represent mean daily minimum (top), mean daily average (middle), and mean daily maximum (bottom) concentrations, with cardinal locations provided (red diamonds). Upstream corresponds to the rights side of the figure and downstream to the left. Rkm refers to river kilometer.

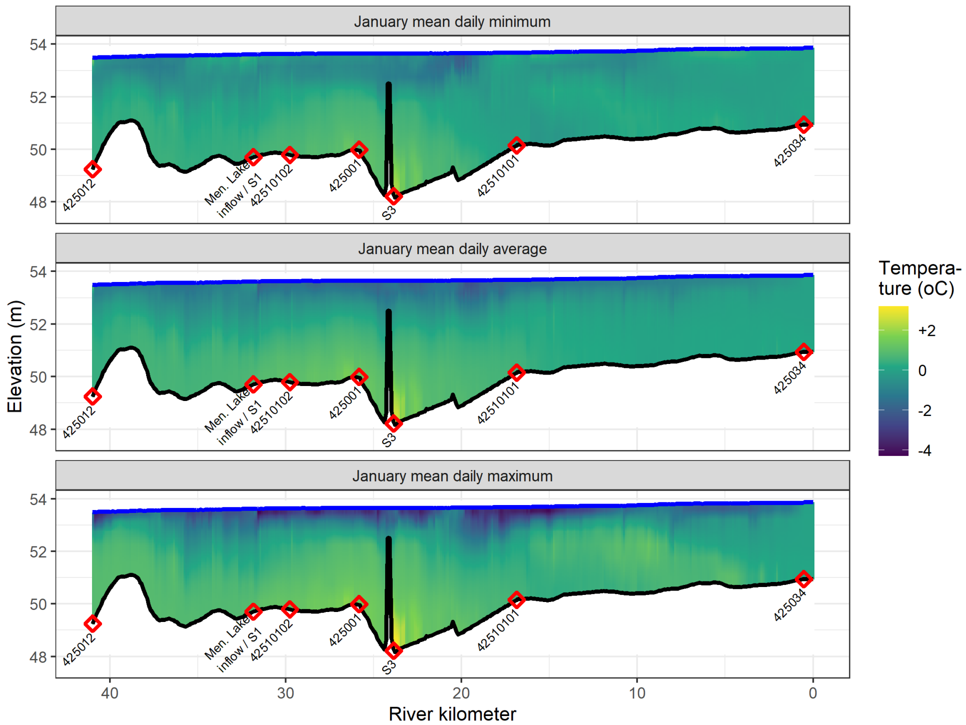

Figure 32. Longitudinal curtain (distance and depth) of the deviation of Flow 2 water temperatures from base water temperatures for SR2 for the month of January. Panels represent mean daily minimum (top), mean daily average (middle), and mean daily maximum (bottom) concentrations, with cardinal locations provided (red diamonds). Upstream corresponds to the rights side of the figure and downstream to the left. Rkm refers to river kilometer.

Table 9. Daily mean DO concentrations in the water column at SR2 for the month of January for all scenarios at selected locations. Red coloured text for scenarios indicates DO concentrations that are less than the base conditions, and blue coloured text indicates concentrations that are greater than the base conditions. Note this table does not include daily minimum or maximum temperatures.

Location	Depth	Base	Climate				Flow		Vegetation	
			1	2	3	4	1	2	1	2
Rkm 16.3 42510101	Surface	5.52	5.19	5.10	5.01	4.59	6.04	5.32	5.51	5.58
	Mid	4.72	4.27	4.17	4.04	3.45	3.58	4.94	4.72	4.74
	Bottom	4.56	4.09	3.99	3.85	3.25	1.91	4.87	4.56	4.57
Rkm 25.3 425001	Surface	5.09	4.80	4.75	4.63	4.26	5.45	4.95	5.10	5.24
	Mid	4.53	4.09	3.99	3.86	3.29	1.55	4.80	4.53	4.56
	Bottom	3.81	3.33	3.23	3.09	2.49	0.03	4.30	3.82	3.82
Rkm 31.3 S1 / L. Menindee	Surface	4.93	4.63	4.57	4.47	4.09	4.40	5.06	4.94	5.17
	Mid	3.97	3.50	3.42	3.27	2.73	1.89	4.46	3.96	4.01
	Bottom	3.85	3.38	3.29	3.14	2.59	1.81	4.39	3.84	3.89
Rkm 40.5 425012	Surface	5.23	4.87	4.79	4.68	4.21	4.84	5.16	5.24	5.28
	Mid	4.76	4.35	4.26	4.14	3.61	1.53	4.97	4.76	4.83
	Bottom	3.97	3.52	3.41	3.28	2.71	0.04	4.47	3.98	4.00

Table 10. Daily mean temperatures in the water column at SR2 for the month of January for all scenarios at selected locations. Red coloured text for scenarios indicates water temperatures that are greater than the base conditions, and blue coloured text indicates water temperatures that are less than the base conditions. Note this table does not include daily minimum or maximum temperatures.

Location	Depth	Base	Climate				Flow		Vegetation	
			1	2	3	4	1	2	1	2
Rkm 16.3 42510101	Surface	30.8	32.4	32.8	33.3	35.6	33.6	29.4	30.6	30.9
	Mid	27.2	28.7	29.2	29.6	31.7	26.7	27.5	27.2	27.2
	Bottom	27.0	28.5	28.9	29.3	31.5	25.1	27.5	27.0	27.0
Rkm 25.3 425001	Surface	32.4	34.1	34.3	34.9	37.1	37.7	30.7	32.3	32.6
	Mid	27.2	28.8	29.2	29.6	31.7	24.6	27.7	27.2	27.3
	Bottom	26.2	27.6	28.0	28.4	30.4	22.2	27.2	26.2	26.2
Rkm 31.3 S1 / L. Menindee	Surface	29.1	30.7	30.9	31.5	33.6	25.4	29.7	29.0	29.3
	Mid	27.8	29.3	29.7	30.1	32.3	23.3	28.2	27.7	27.9
	Bottom	27.8	29.2	29.7	30.1	32.3	23.3	28.1	27.7	27.8
Rkm 40.5 425012	Surface	30.2	31.8	32.1	32.7	34.9	31.5	29.7	30.1	30.3
	Mid	28.5	30.1	30.5	30.9	33.2	24.5	28.5	28.4	28.5
	Bottom	27.1	28.6	29.0	29.4	31.5	22.0	27.7	27.1	27.1

Time series

Time series plots of DO (Figure 33) and temperature (Figure 36) are presented for the base case for the months of December and January at selected locations. The largest increases in DO concentrations at SR1 were predicted for vegetation scenario 2 at all depths and locations and by a large margin compared to the changes in DO concentration for the other scenarios, which resembled base conditions, and with smaller deviations. Water temperature at all depths at SR2 were most affected by air temperature changes related to the climate scenarios, with climate scenario 4 demonstrating the largest increase in water temperatures from base conditions. Very low flows at SR2 resulted in decreased variability of temperatures, particularly in the metalimnion (middle of the water column) and included some of the lowest modelled temperatures in the metalimnion throughout the modelling period. The last time series we report on is chlorophyll *a* at SR1 (Figure 37). We present this data for both vegetation scenarios to provide context in the discussion section for the temperature and DO results at SR1. Chlorophyll *a* was approximately the same for base conditions and vegetation scenario 2, however, it increased by as much as 50% in scenario 2 at some locations by the end of the modelling period.

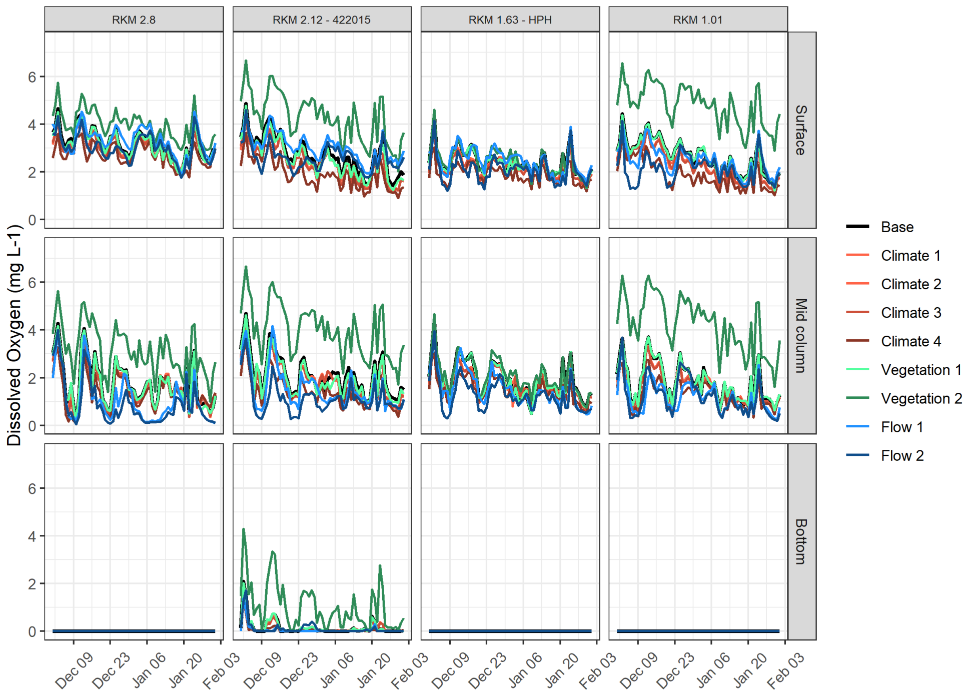

Figure 33. Scenario time series of daily mean DO concentrations at selected locations at SR1 from 01/12/2019 to 01/02/2020. Sites proceed from upstream on the right to downstream on the left. RKM refers to river kilometre.

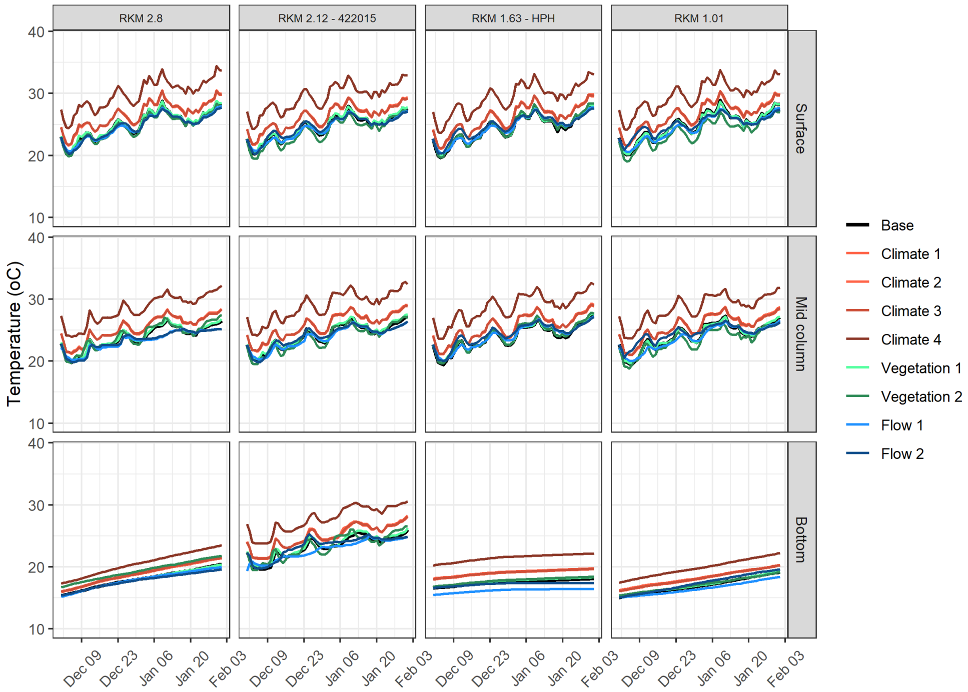

Figure 34. Scenario time series of daily mean water temperatures at selected locations at SR1 from 01/12/2019 to 01/02/2020. Sites proceed from upstream on the right to downstream on the left. RKM refers to river kilometer.

Figure 35. Scenario time series of daily mean DO concentrations at selected locations at SR2 from 01/01/2024 to 01/03/2024. Sites proceed from upstream on the right to downstream on the left. RKM refers to river kilometer.

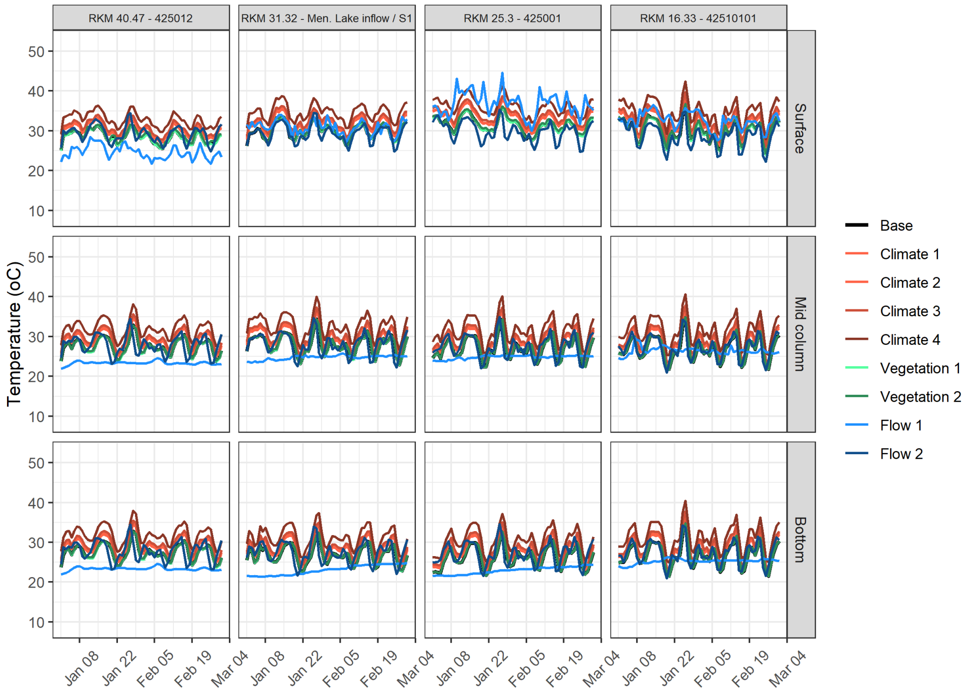

Figure 36. Scenario time series of daily mean water temperatures at selected locations at SR2 from 01/01/2024 to 01/03/2024. Sites proceed from upstream on the right to downstream on the left. RKM refers to river kilometer.

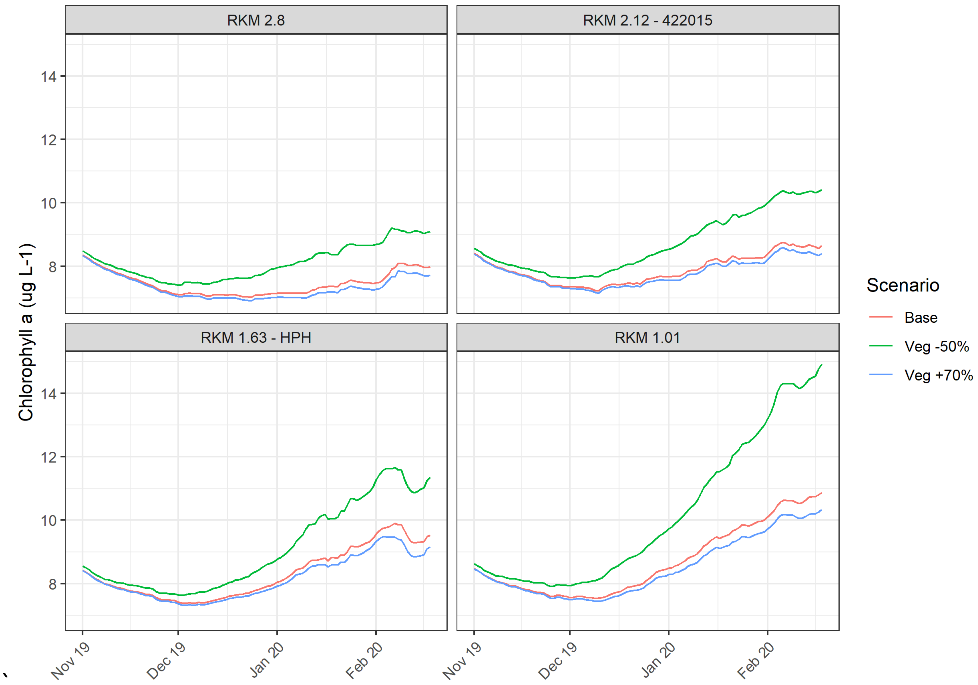

Figure 37. Time series of daily mean chlorophyll a concentrations at selected locations at SR1 for base and vegetation scenarios from 01/11/2019 to 18/02/2020. RKM refers to river kilometer.

Water column stability

Water column stability is presented as Schmidt's stability index for SR1 (Figure 38), and the difference in water temperature between the top and bottom of the water column for SR2 (delta T; Figure 39) at selected locations in the model. Schmidt's stability tended to be greater in deeper water, however, at the HPH station and the gauge 422015, the water depth is similarly shallow, with Schmidt's stability more than twice as great at certain times of the modelling period. The site with the greatest Schmidt's stability throughout the modelling period was at river kilometre (rkm) 1.01. The climate scenarios showed the greatest stability, however, the flow scenarios dominated stability in the latter months depending on when the flushing flows were discharged.

At SR2, flow scenario 1 demonstrated higher delta T in the upper parts of the reach and early in the modelling period (Figure 39), while flow scenario 2 provided a lower bound for delta T in general. At the lowest point in the reach (425012), flow scenario 1 delta T values were lower than the other scenarios. Flow scenarios aside, the delta T values were typically similar between scenarios with minor variations compared with the flow scenarios, with climate scenario 4 demonstrating the highest delta T values, and the vegetation scenarios demonstrating the lowest.

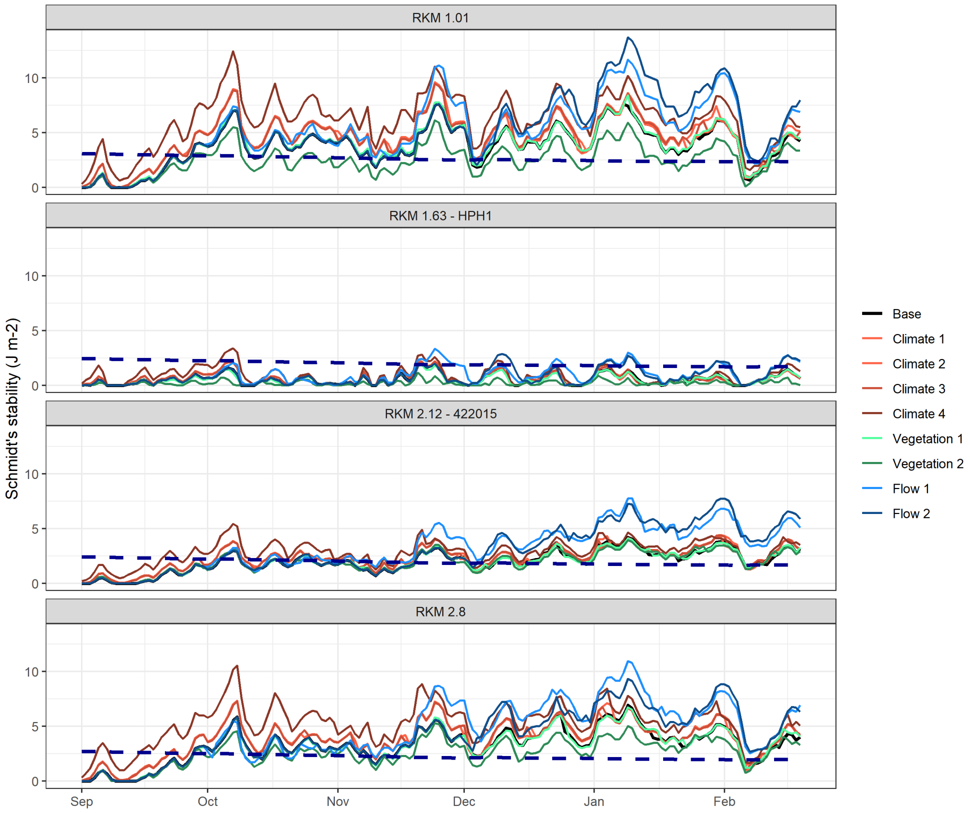

Figure 38. Scenario time series of Schmidt's stability index for selection locations at SR1 during the modelling period. The dashed blue line indicates the base condition depth of water at that location and time. RKM refers to river kilometer

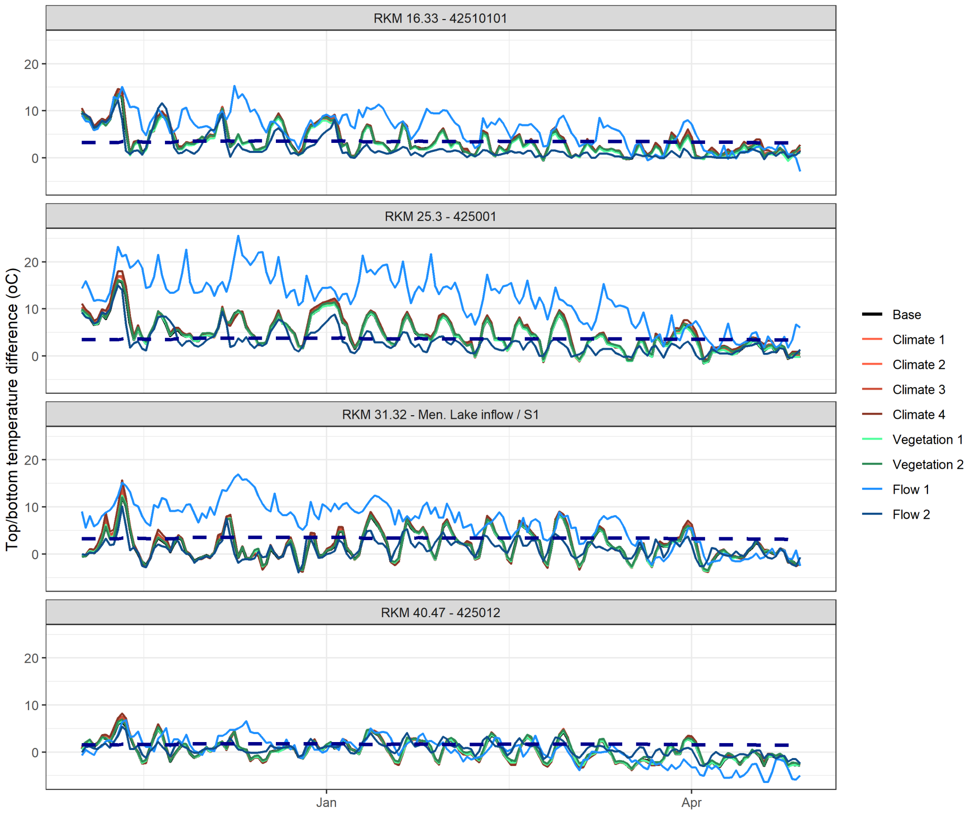

Figure 39. Scenario time series of top and bottom water temperature differences for selection locations at SR2 during the modelling period. The dashed blue line indicates the base condition depth of water at that location and time. RKM refers to river kilometer.

Fish Habitat Suitability Index

Fish habitat suitability was estimated for both study reaches and for three species of fish: carp, Golden perch, and Bony bream. Murray cod demonstrate similar physiological response to Bony bream (Zhai et al 2022), hence results for bream can be used as a surrogate for cod.

At SR1, habitat was unsuitable in the hypolimnion for base conditions (Figure 40), typically, with environmental conditions and fish physiology determining the height in the water column that unsuitable habitat extended to from the bottom. Habitat suitability decreased toward the end of the modelling period when temperature increased and water level decreased. Deeper water exhibited smaller volumes of suitable habitat as a function of the depth of water, however the threshold between suitable and unsuitable habitat occurred at the same elevation, irrespective of the depth of water. The total volume of suitable habitat in the waterhole was greatest for carp and least for Bony bream (Figure 42), with a global constriction of suitable habitat for all species as the modelling period progresses. Climate scenario 4 appeared to reduce the habitat the most, while the flow scenarios decreased the habitat the least, especially after October and December for flow scenarios 1 and 2 respectively.

At SR2, suitable habitat was present throughout the model domain (Figure 41), and throughout the modelling period with the exception of pockets of unsuitable habitat occurring at the surface of the water, the longest and deepest of which occurs at the end of December. climate scenario 4 (Figure 43) reduces habitat the most, expanding the base scenario pockets of unsuitable habitat in both space and time. Flow scenario 1 decreased habitat consistently through the months of December and March, reducing the bream and perch habitat to approximately 75 percent of the total water volume in the model domain.

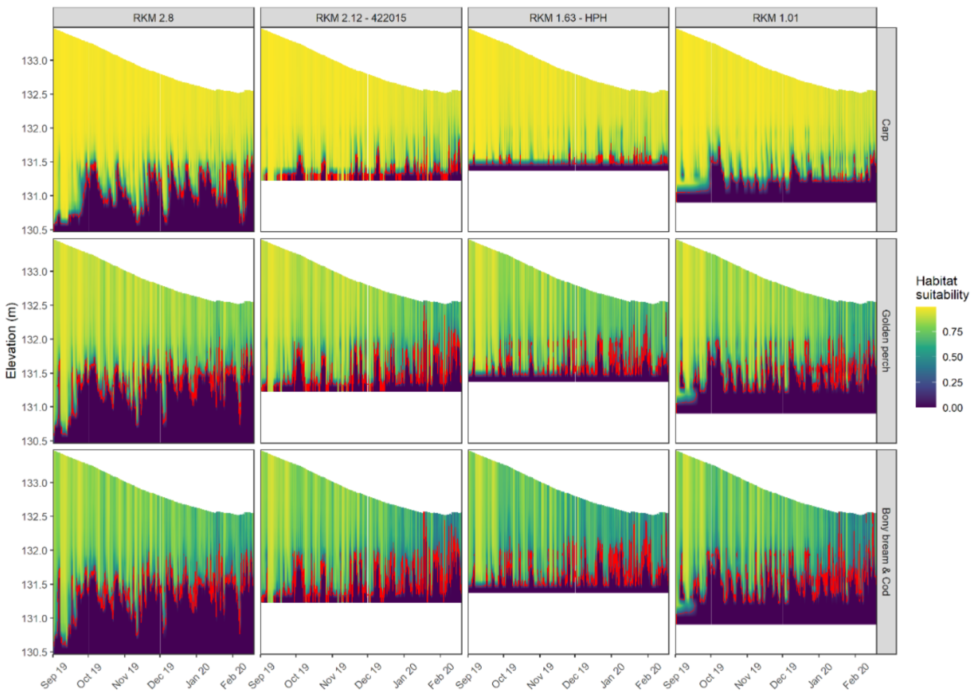

Figure 40. Fish habitat suitability as a function of time and depth at SR1 under base conditions at key locations. Unsuitable habitat at less than the index of 0.2 is shown in blue with the cutoff between suitable and unsuitable indicated by the red line. RKM refers to river kilometer.

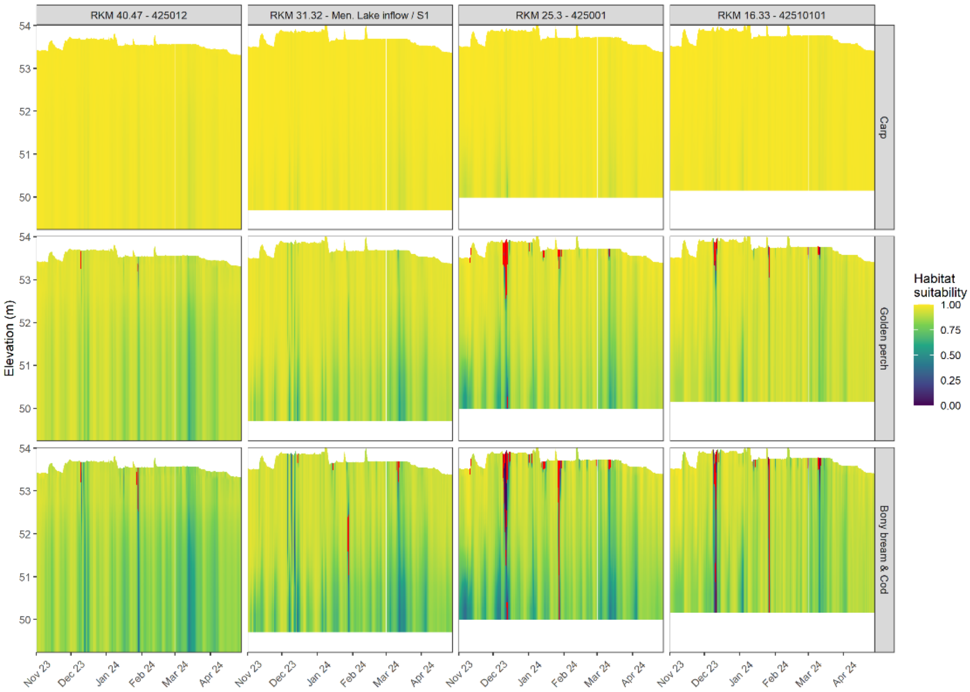

Figure 41. Fish habitat suitability as a function of time and depth at SR2 under base conditions at key locations. Unsuitable habitat at less than the index of 0.2 is shown in blue with the cutoff between suitable and unsuitable indicated by the red line. RKM refers to river kilometer.

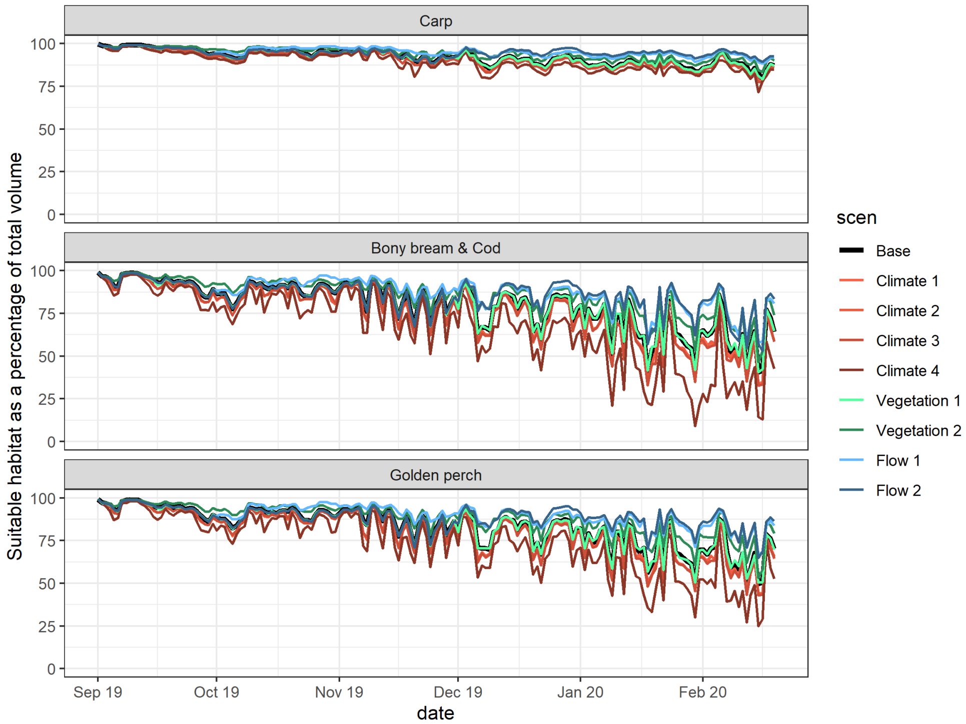

Figure 42. Time series of suitable habitat at SR1 as a percentage of total waterhole volume by species for the entire modelling period.

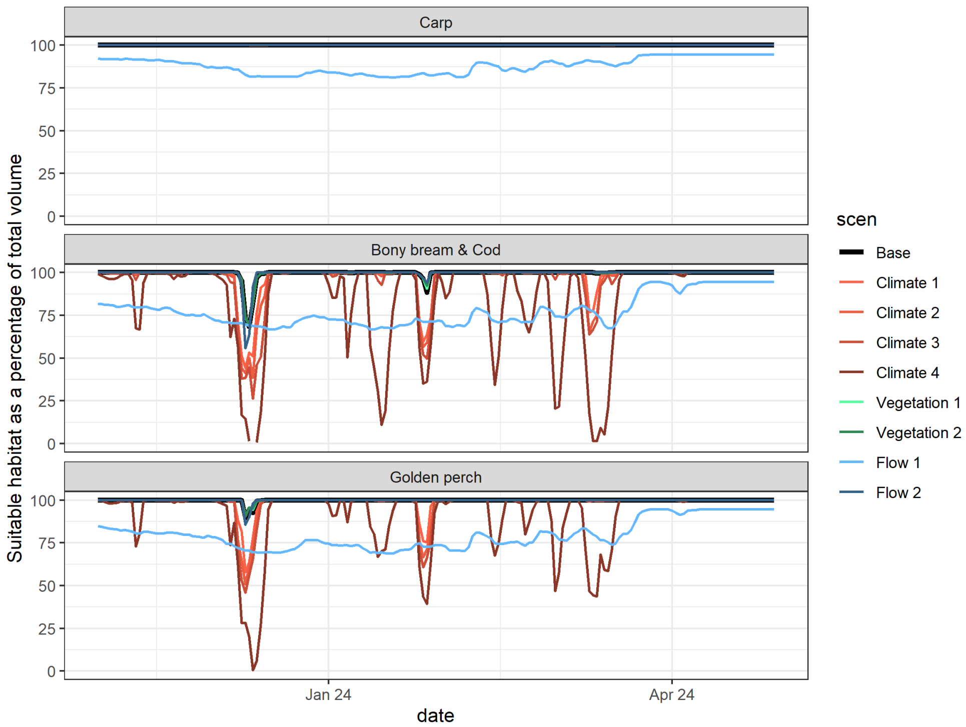

Figure 43. Time series of suitable habitat at SR2 as a percentage of total waterhole volume by species for the entire modelling period

Variable catalogue and correlations

The information in the previous sections seeks to illustrate how the systems respond to specific environmental conditions. In this section we take a broader approach and look at the relationship between some of the variables mentioned previously. We provide two sets of general information: (1) a catalogue of the variables within the systems (Table *11*) and general range of values (10th, 50th, and 90th percentiles) for each study reach, and (2) matrices of the Spearman correlation coefficients for SR1 (*Table 12*) and SR2 (*Table 13*).

Comparison of the two systems indicates SR1 is physically smaller in all dimensions than SR2 (Table *11*). SR1 has taller and more dense vegetation lining its banks, providing more shade from solar radiation. Velocity, a possible surrogate for flow rate, indicates SR2 was far more hydrodynamic than SR1. Water temperature and DO were generally lower in SR1, as was suitable habitat for each of the fish species considered.

As an indicator variable, air temperature was related to many of the other variables, and comprised some of the strongest relationships presented in the correlation tables for both study reaches (Table *12*) and *(Table 13*).

At SR2, only water temperature was correlated more strongly with DO than air temperature. Vegetation characteristics showed essentially no correlations to DO, temperature, as well as habitat for both st udy reaches, even though they showed weak to moderate correlations compared with other variables t hat affect temperature and DO, such as effective shade and shortwave radiation,

Height in the water column, along with air temperature, water temperature and DO, were strongly correlated with habitat suitability for all of the fish species for both study reaches, while velocity was also related to habitat at SR1. Morphological features affected fish habitat differently at each site. Whereas greater volume indicated improvements in habitat at SR1, the opposite appeared to be the case at SR2, with increases in depth, width and cross-sectional area resulting in decreases in habitat. Fish habitat was more strongly correlated to weather conditions at SR1 than at SR2.

Table 11. Variable catalogue of system parameters and 10th, 50th, and 90th percentile values for each study reach. The abbreviations are how the variables are displayed in subsequent tables.

Abbreviation	Variable	Study Reach 1 - Culgoa			Study Reach 2 - Darling		
		10th %-ile	50th %-ile	90th %-ile	10th %-ile	50th %-ile	90th %-ile
-	Number of 3D cells	3	6	11	6	7	9
zCll	Cell height in water column (i.e., elevation) (m)	131	132	133	50	52	54
Dist	Distance along reach (m)	-	-	-	-	-	-
Aspc	Stream aspect (° clockwise from North)	-	-	-	-	-	-
D	Water depth (m)	0.64	1.44	2.12	2.92	3.69	4.49
wTop	Top width (m)	18.4	26.6	36.7	31.4	38.9	48.0
aXsc	Cross sectional area (m^2)	9.1	27.5	50.3	50.6	93.2	152.2
vegH_RR	Mean vegetation height on the right bank (m)	3.3	6.2	10.9	0.1	3.8	14.7
vegH_RL	Mean vegetation height on the left bank (m)	2.8	6.0	11.1	0.1	3.6	12.3
vegD_RR	Mean vegetation density on the right bank (%)	0.35	0.55	0.85	0.05	0.35	0.9
vegD_RL	Mean vegetation density on the left bank (%)	0.3	0.55	0.85	0.05	0.3	0.85
tAir	Air temperature at water surface (°C)	19.0	26.5	33.4	17.2	25.2	31.3
Swr	Shortwave radiation at water surface (W m^{-2})	855	1754	2664	1497	2802	3789
w10	Wind speed at 10 m (m s^{-1})	1.39	2.12	3.01	0.82	1.38	2.29
Es	Effective shade (%)	2.8	24.3	62.0	0.5	12.4	53.8
V	Horizontal velocity (m s^{-1})	0.0002	0.0029	0.0127	0.0212	0.0998	0.1861
TEMP	Water temperature (°C)	12.1	19.9	26.2	18.6	25.9	31.2
DO_MGL	Dissolved oxygen (mg L^{-1})	0.23	2.33	5.03	3.38	5.17	6.55
SSI	Schmidt's stability index (J m^{-2})	0.00	0.34	2.17	-	-	-
dltT	Top-bottom temperature difference (°C)	-	-	-	0.10	2.35	7.39
HSI_carp	Habitat suitability - carp (-)	0.35	0.94	0.98	0.97	0.99	0.99
HSI_bream	Habitat suitability - bream and cod (-)	0.00	0.56	0.83	0.74	0.89	0.94
HSI_perch	Habitat suitability - perch (-)	0.00	0.70	0.90	0.85	0.94	0.97

Table 12. Variable correlation matrix for base conditions at SR1. Numbers within the cell show the strength of the correlation between two variables, and the colour of the cells indicates positive (blue) or negative (red) correlation. Table 10 for definition of the abbreviated variable names. tAIR is air temperature, swr is shortwave radiation, w10 is wind speed 10 m above the topographic surface, es is calculated evaporative loss, V is water velocity, TEMP is water temperature, DO is dissolved oxygen, SSI is Schmidt stability index, Es is effective shard, HIS is habitat suitability index, vegH is mean vegetation height (right and left), vegD is percentage vegetation density (right and left),

		Indicator and response								**Response only**		
		tAir	swr	w10	Es	V	TEMP	DO_MGL	SSI	HSI_carp	HSI_bream	HSI_perch
Indicators	zCll	*NA*	*NA*	*NA*	*NA*	0.20	-0.01	0.52	-0.38	0.52	0.53	0.53
	Dist	0.01	0.23	0.01	-0.20	0.19	0.05	0.06	0.29	0.09	0.09	0.09
	Aspc	0.00	0.02	-0.01	-0.04	0.02	0.02	0.01	0.06	0.02	0.01	0.01
	D	*NA*	*NA*	*NA*	*NA*	0.26	-0.50	0.28	0.50	0.26	0.26	0.26
	wTop	*NA*	*NA*	*NA*	*NA*	0.20	-0.29	0.18	0.33	0.17	0.17	0.17
	aXsc	*NA*	*NA*	*NA*	*NA*	0.25	-0.46	0.27	0.46	0.25	0.25	0.25
	vegH_RR	0.00	-0.15	-0.02	0.14	-0.11	-0.03	-0.01	-0.11	-0.02	-0.02	-0.02
	vegH_RL	0.00	-0.27	0.00	0.35	-0.08	-0.05	0.04	-0.11	0.02	0.02	0.02
	vegD_RR	0.00	-0.11	-0.01	0.10	-0.08	-0.03	-0.01	-0.08	-0.03	-0.02	-0.02
	vegD_RL	0.00	-0.21	0.00	0.30	-0.08	-0.03	0.03	-0.13	0.01	0.02	0.01
	tAir		0.38	0.27	-0.07	-0.08	0.79	-0.44	0.29	-0.35	-0.37	-0.37
	Swr			0.01	-0.59	0.07	0.43	-0.24	0.35	-0.17	-0.18	-0.18
	w10				-0.01	0.28	0.18	0.14	-0.04	0.15	0.16	0.16
	Es					-0.11	-0.13	0.07	-0.21	0.03	0.04	0.04
	V						-0.01	0.49	0.16	0.53	0.53	0.53
	TEMP							-0.39	0.14	-0.28	-0.30	-0.29
	DO_MGL								-0.19	0.96	0.99	0.98
	SSI									-0.13	-0.15	-0.14

Table 13 Variable correlation matrix for base conditions at SR2. Numbers within the cell show the strength of the correlation between two variables, and the colour of the cells indicates positive (blue) or negative (red) correlation. See Table 11 and 12 for definition of the abbreviated variable names.

		Indicator and response								Response only		
		tAir	swr	w10	Es	V	TEMP	DO_MGL	dltT	HSI_carp	HSI_bream	HSI_perch
Indicators	zCll	*NA*	*NA*	*NA*	*NA*	0.26	0.28	0.44	-0.05	0.59	0.52	0.55
	Dist	0.00	-0.02	0.00	0.01	0.08	0.08	-0.24	0.08	-0.21	-0.21	-0.21
	Aspc	0.00	0.02	-0.01	-0.06	-0.12	0.00	-0.01	0.11	0.00	-0.01	-0.01
	D	*NA*	*NA*	*NA*	*NA*	-0.17	0.15	-0.23	0.21	-0.16	-0.18	-0.17
	wTop	*NA*	*NA*	*NA*	*NA*	-0.27	0.07	-0.10	0.21	-0.06	-0.07	-0.06
	aXsc	*NA*	*NA*	*NA*	*NA*	-0.29	0.08	-0.11	0.25	-0.06	-0.08	-0.07
	vegH_RR	0.00	-0.12	-0.02	0.17	0.07	0.01	-0.02	-0.03	-0.02	-0.02	-0.02
	vegH_RL	0.00	-0.09	-0.01	0.19	0.04	0.00	0.01	-0.02	0.01	0.01	0.01
	vegD_RR	0.00	-0.12	-0.01	0.17	0.05	0.01	-0.02	-0.02	-0.02	-0.02	-0.02
	vegD_RL	0.00	-0.08	0.00	0.17	0.03	0.00	0.00	-0.01	0.00	0.00	0.00
	tAir		0.31	-0.02	-0.08	0.23	0.67	-0.45	0.41	-0.19	-0.27	-0.23
	swr			-0.08	-0.45	0.03	0.27	-0.05	0.39	0.09	0.05	0.07
	w10				-0.01	0.03	-0.05	0.03	-0.19	0.09	0.09	0.10
	Es					0.02	-0.08	0.03	-0.13	-0.01	0.00	0.00
	V						0.27	-0.04	-0.30	0.08	0.07	0.08
	TEMP							-0.52	0.11	-0.18	-0.30	-0.24
	DO_MGL								-0.02	0.87	0.91	0.90
	dltT									0.05	0.03	0.03

Discussion

Riparian Vegetation

The riparian vegetation model functioned as a means of characterising the localised sheltering along the waterway, particularly shading of radiation and reduction of wind speeds at the water surface, which was similarly observed by Zhai et al. (2023). From this study, the links between vegetation characteristics and shading by vegetation were apparent for SR1 (Figure 14 and Figure *16*), where vegetation height and density were greatest at the upstream end and middle of the reach, resulting in the greatest shade and lowest incoming radiation.

While estimates of vegetation and shading were considered representative for the model application, field validation of canopy density, and its effect of reductions in solar penetration and wind sheltering would assist in reducing the uncertainty of relationships of sheltering by vegetation, and the effects on temperature, dissolved oxygen and other water quality variables. There is substantial evidence (e.g., Klos & Link, 2018) to indicate an important role for riparian vegetation in surface water temperature, and thereby dissolved oxygen. The certainty and degree to which vegetation modulates water quality requires field observations to fully calibrate the shading model, noting the antagonistic relationship of wind sheltering and solar shading from vegetation, i.e., shading likely to decrease surface water temperature and sheltering to reduce mixing and therefore maintain warmer water at the surface.

Model calibration

Modelling is not an exact science, but if the information used is accurate and sufficient, and the algorithms used are generally representative of the processes occurring, modelling can have at least three beneficial outcomes: (1) it can replicate historical conditions with some accuracy (see Section 0) in order to estimate future conditions, (2) it can be used to infer how conditions will change based on changes to the environment through scenario analysis (see Section 0) and (3) it can be used to infer other processes not included in the model based on where inaccuracies in model simulations can be identified. The first two points are the subject of the discussion in this section and the one that follows. The third point is discussed in various parts of the following discussion.

SR1 – Culgoa River at Brenda

The model calibration process demonstrates the complex and dynamic nature of the river system. It is subject to many internal (e.g., shading within the water column) and external (e.g., shading from vegetation) factors. For example, at SR1, the monitoring data show that DO concentrations near the surface decrease steadily throughout the modelling period. As water levels fall below 1.25 m, at the beginning of 2020, productivity appears to increase substantially, resulting in the large diurnal swings in DO, and doubling the daily maximum DO concentrations at the surface. Near the end of January conditions at the HPH profile chain went anoxic. Temperatures during this time increased, thereby reducing DO solubility, but even a brief cooling event prior to the anoxic event wasn't sufficient in stimulating productivity. Temperature has been suggested to play a strong role in blackwater events (Vithana et al., 2019), and is a critical parameter for sediment oxygen demand in the model (BMT, 2023b).

These dynamics suggest the system is possibly chaotic—that small differences in initial and boundary conditions can cause quantum changes in state with few, if any, indicators of that change. It is also possible that other processes are occurring that have not been or cannot be accounted for, such as reduced atmospheric exchange as a result of high sediment and organic matter concentrations. In terms of atmospheric exchange of oxygen with the water column, the Tuflow FV model does not account for the interference of sediment (Zahraeifard & Deng, 2012); hence, the model predicted oxygenation at the water surface in late January and February, when the monitoring data show clearly this did not occur. With that said, we believe the model performed adequately in predicting DO concentrations, especially in the mid-depths of the water column. It captured most of the dynamics and disturbance resulting from changing environmental conditions and is sufficient to estimate existing conditions and the changes to those estimates when the conditions change.

The model performed well in terms of temperature, but only after modifying the shortwave radiation to account for high suspended sediment concentrations. The data to verify that sediment concentrations were elevated at the time of the monitoring were not available, however, anecdotal accounts indicate the Culgoa is often very turbid under normal conditions. Sediment combined with phytoplankton and cyanobacteria block short wave radiation from penetrating water column beyond epilimnion with reductions in shortwave penetration to lower depths of 50-65%.

SR2 – Darling River at Menindee Lakes

Like SR1, the model accurately predicted water temperature. In terms of DO, the model performance for 425012 is similar to that of SR1. Surface predictions of DO at the two stations with depth profile measurements (42510101 & 42510102; Figure 20 & Figure 21) show significant productivity near the surface that the model does not replicate. The reasons for this might include discrepancies between productivity within the model and phytoplankton concentrations coming from inflows. The differences in the modelled and observed diurnal DO swings (i.e., daily maximum and daily minimum DO) show productivity that was not simulated by the model. Nevertheless, in the metalimnion and hypolimnion, the dynamics of DO were captured well enough to make estimates of changes based on changing environmental conditions. Median modelled velocities throughout the model domain were around 0.1 m s^{-1}, with some sections of the reach above 0.2 m s^{-1}. Flow velocity recommendations to minimise cyanobacterial blooms for the Darling River at Menindee promulgated a minimum velocity of 0.05 m s^{-1} (Facey et al., 2021) to minimise stratification and the risk of blooms.

Scenarios

We constructed scenarios that provided a snapshot of hypoxic and anoxic water quality outcomes based on possible conditions and controls to understand the drivers of water quality within the Murray-Darling Basin. These scenarios were developed primarily to assess the effects of climate change on stratification, flow regulation or localised modification of riparian vegetation density. The scenarios did not consider secondary effects including climate change effects on the hydrology or other factors (e.g., bush fires, regulations) that could, for example, alter the riparian vegetation. These factors were beyond the scope of the present study but could be considered as part of a more detailed set of scenarios that introduce a range of socio-economic factors as drivers of potential future scenarios.

Climate change

Air temperature was one of the most important drivers of both water temperature and DO changes for all scenarios, as shown through the climate scenarios, and through the variable correlations. Given that stream temperature is highly correlated with air temperature (Kaushal et al., 2010; Isaak et al., 2012), which for the climate scenarios are as much as 25% greater than base conditions, stream temperatures are expected to rise significantly, thereby decreasing DO, in-part, through decreased gas solubility. While higher temperatures add energy for thermocline stabilization with the potential to create pockets of refugia, the water is generally too warm with not enough oxygen to support threatened fish species. This was evident in the habitat suitability estimations, particularly for Bony bream and Murray cod at SR1, where metalimnion and hypolimnion temperatures reached high 20 degrees and low 30 degrees in January (Table 8), and suitable habitat areas dropped to less than 25% of the available waterhole volume.

Vegetation modification

The vegetation scenarios presented some interesting implications for managing these dryland rivers and waterholes. There were divergent dynamics under these scenarios that will require more careful investigations, if they are to be seriously considered as strategies for mitigating risks to fish populations.

Firstly, we examined the results largely in terms of distance along the river and depth, assuming both rivers were laterally homogeneous, however, we acknowledge the possibility refugia might exist within these margins (Ebersole et al., 2003). The development of the model was conducted for increased resolution over the HPH models, however, the need for computational efficiency constrained the practical limits of higher lateral resolution. In this regard, morphology and riparian vegetation play significant roles.

Vegetation clearing (vegetation scenario 2) resulted in greater radiation reaching the surface of the water and increased productivity, and therefore higher DO on average. Greater productivity was associated with algal biomass which in turn limited light penetration to lower depths and cooled the water down. The interactions among phytoplankton, DO and turbidity are complex and affect DO concentrations over extended time scales as well as the diurnal variations in DO. For example, increased algal biomass will be associated with greater diurnal swings in DO increased likelihood of anoxia. The Tuflow FV model redistributes shortwave energy at each vertical layer in the model based on absorption by phytoplankton (BMT, 2023b).

The second finding relates to the first finding with less productivity from increased shading in some locations resulting in more light penetration to lower depths. Vegetation scenario 1 showed decreased temperatures in the epilimnion, but increased temperatures at lower depths, where productivity is not likely to occur. Slight increases in DO were observed for both vegetation scenarios at SR2, indicating that cooler temperatures increased dissolved gas solubility for vegetation scenario 1 and productivity increasing production of DO for vegetation scenario 2. This is consistent with slight temperature decreases in vegetation scenario 1, and slight increases in temperature for vegetation scenario 2.

Vegetation scenario 2 assumes clearing of riparian vegetation, which presents the appearance of improved water quality through increased DO, however, we do not endorse the clearing of vegetation as a management strategy although riparian vegetation can also be lost through bushfires. Riparian vegetation loss via clearing or bushfires has other negative impacts on water quality that bear consideration. For example, Beavis et al. (2023), found erosion and debris flows from vegetation loss through bushfires contributed to extended periods of high turbidity. Bunn et al. (1999) showed riparian disturbances resulted in significant loss of ecosystem function.

Flow regulation

The difference in hydrology of the two study reaches offers some insights into how flows, or lack thereof, influence the water quality, and potentially habitat. SR1 which was dry during the period of study, offers the opportunity to examine inflows that create new conditions. While generally always flowing, SR2 has had periods of very low flows which have been associated previously with impaired water quality. For the FSR2 site, a deeper understanding is possible of the way in which drought and flow regulation impact water quality.

At SR1 two flow events were introduced at two different times, and in both cases, DO generally decreased, except at the surface (Table 7), while temperatures dropped very slightly (Table 8). Higher

DO at the surface was likely due to enhanced productivity, while the lower DO in the metalimnion and hypolimnion was likely due to deeper water, re-entrained or introduced sediment, and diminished light at those depths. Conditions were slightly more favourable for flow scenario 1 because it has there was more time for the sediment to settle out.

At SR2, flow scenarios were operationally opposite, with very low flows forming one end of the spectrum and twice the observed discharge forming the other. Flow scenario 1 demonstrated higher DO in the epilimnion especially in the upper reaches, likely due to productivity, however oxygen demand and slow-moving waters increased the intensity of stratification, trapping the colder, deoxygenated waters at lower depths. This is consistent with findings of Mitrovic et al. (2011), who found velocities of greater than 0.03 m s^{-1} were necessary to create sufficient mixing conditions. Because median velocities are less than 0.021 m s^{-1} for this scenario at SR2, exchange between the upper and lower layers was inhibited (Mallen-Cooper & Zampatti, 2020).

We note at this point that flow scenarios introduce uncertainty which cannot be resolved or minimised without further monitoring and possibly pilot studies. The reason for this is that inflows carry nutrients, sediment, organic matter and other constituents (including DO), the concentrations of which are unknown. The source of those inflows becomes critical for managing water quality, especially for blackwater events or cyanobacterial blooms. Our flow scenarios assumed the inflow water quality did not change from base conditions. This creates the understanding of how flow alone affects water quality and does not consider inflow mass loads and the introduction of that mass for ecological processes within the system. This is acceptable for circumstances for which factors such as velocity are the important parameters, and possibly circumstances where low flows simply occur under diminishing upstream input.

Data catalogue and correlations

The catalogue of variables, their ranges and correlations, present another way of looking at the large amount of information the models produce. Some of these variables can be managed, such as vegetation and flow regulation, whereas others cannot. Air temperature plays a large part in all of the dynamics of the model (*Table 12* & *Table 13*) but management of even local climate is more challenging.

Vegetation has been shown to be effective at modulating climatic factors (Davies-Colley et al., 2000), but the findings within this report indicate that the level of moderation might not offset the impacts that rising air temperature will have on DO and water temperature. Morphology also plays a role, as some results from this study indicate, and those of other studies (Quinn & Wright-Stow, 2008). Interestingly, morphology appeared to affect water temperatures differently between the two study reaches. At SR1, greater volume in the waterhole (width and depth) resulted in lower temperatures and higher DO concentrations, and at SR2, the opposite was the case, though the correlations observed for SR2 were generally less strong. The Culgoa River at Brenda is generally narrower and shallower than the Darling River at Menindee and the lack of mixing allows for stratification and for the lower depths to remain cooler. Suspended sediment plays a role in reducing solar input, attenuating a large proportion of radiation, heating the upper waters, and increasing the strength of stratification, but as sediment settles out as the water level decreases, there is greater solar penetration.

Study limitations and opportunities

The model presented in this report represents a robust tool, constructed with state-of-the-art modelling software combined with fit-for-purpose data sets. We have validated the model using the monitoring data; we believe it is capable of manifesting change in water quality conditions based on the environmental context. The model is a useful tool for the purposes it was designed, however it comes with some constraints.

The first disclaimer is that the model can estimate water quality based on known conditions, but it cannot predict the future conditions (i.e., more forcing data). In addition, we highlight some factors that could be important, but were not incorporated into the modelling at this time:

- While geomorphology was considered in a general way, the degree to which geomorphology impacts water quality could be significant, especially considering phenomena such as entrenchment or sediment transport (Tibby et al., 2023). Information regarding sediment for these systems remains a data gap.
- Nutrient biogeochemistry was addressed in a general way in the model, to the degree the data permitted, though it is likely a significant driver of internal processing of nutrients, carbon and organic matter in isolated waterholes, such as the Culgoa River at the Brenda weir pool (Townsend & Edwards, 2003).
- Modification of riparian vegetation has the potential to impact in-stream nutrients and organic matter. We assumed for this study that revegetation or clearing was small relative to the overall sources of nutrients and organic matter, but this is an unknown.
- While larger, wider rivers may reduce the influence of riparian vegetation on in-stream temperatures (Quinn & Wright-Stow, 2008), the role of vegetation may still be important in such systems by providing refugia near the stream banks.
- While the LiDAR point clouds provided immense amounts of detailed information on the nature of riparian vegetation characteristics, validation of vegetation microclimate effects would be an important data gap to address.

Conclusions

The water quality modelling presented in this report represents an expansion of the modelling efforts started with the HPH project to develop a tool capable of simulating water quality conditions in rivers of the Murray-Darling Basin. The HPH project identified extended periods of anoxia in bottom waters of waterholes, sometimes extending to surface waters, with absence of flow and declining water levels. The waterholes are important fish refugia during cease-to-flow period. The 3D model used in our study leverages continuous measurements of dissolved oxygen and temperature at various water column depths; high-resolution LiDAR data to characterize riparian vegetation; and sophisticated modelling methods to assess and demonstrate the impacts of changing environmental conditions on water quality over two selected river stretches. The model results provide a greater understanding of the dynamics of river water quality under variable flow conditions and connections between flowing waters, isolated waterholes, riparian areas, as well as regional and global climatic conditions. The model is suitable as a tool to test different management options to maintain fish habitat under various flow conditions, including specific weather events like heat waves or storms, as well as the changes expected as climate change intensifies, and warming and stratification become more frequent for a given management regime.

References

Anbumozhi, V., Radhakrishnan, J., & Yamaji, E. (2005). Impact of riparian buffer zones on water quality and associated management considerations. Ecological Engineering,

Aslam, Z., Chow, C. W. K., Murshed, F., Van Leeuwen, J. A., Drikas, M., & Wang, D. (2013). Variation in character and treatability of organics in river water: An assessment by HPAC and alum coagulation [Article]. *Separation and Purification Technology*, *120*, 162-171. https://doi.org/10.1016/j.seppur.2013.09.033

Australia, G. (2014). *LiDAR Upper Darling 2013-2014*.

Australia, G. (2019). *Menindee Lower Darling LiDAR*.

Beavis, S. G., Wong, V. N. L., Mosley, L. M., Baldwin, D. S., Latimer, J. O., Lane, P., & Lal, A. (2023). Water quality risks in the Murray-Darling basin [Article]. *Australian Journal of Water Resources*, *27*(1), 85-102. https://doi.org/10.1080/13241583.2022.2163475

Bernot, M. J., Sobota, D. J., Hall, R. O., Mulholland, P. J., Dodds, W. K., Webster, J. R., Tank, J. L., Ashkenas, L. R., Cooper, L. W., Dahm, C. N., Gregory, S. V., Grimm, N. B., Hamilton, S. K., Johnson, S. L., McDowell, W. H., Meyer, J. L., Peterson, B., Poole, G. C., Maurice Valett, H. M., Arango, C., Beaulieu, J. J., Burgin, A. J., Crenshaw, C., Helton, A. M., Johnson, L., Merriam, J., Niederlehner, B. R., O'Brien, J. M., Potter, J. D., Sheibley, R. W., Thomas, S. M., & Wilson, K. (2010). Inter-regional comparison of land-use effects on stream metabolism [Article]. *Freshwater Biology*, *55*(9), 1874-1890. https://doi.org/10.1111/j.1365-2427.2010.02422.x

BMT. (2023a). *Tuflow FV Science Manual*.

BMT. (2023b). *TUFLOW FV Water Quality (WQ) Module User Manual*.

Boyd, M., & Kasper, B. (2003). *Analytical Methods for Dynamic Open Channel Heat and Mass Transfer Methodology for the Heat Source Model Version 7.0.*

Bunn, S. E., Davies, P. M., & Mosisch, T. D. (1999). Ecosystem measures of river health and their response to riparian and catchment degradation [Article]. *Freshwater Biology*, *41*(2), 333-345. https://doi.org/10.1046/j.1365-2427.1999.00434.x

Bunn, S. E., Thoms, M. C., Hamilton, S. K., & Capon, S. J. (2006). Flow variability in dryland rivers: Boom, bust and the bits in between [Article]. *River Research and Applications*, *22*(2), 179-186. https://doi.org/10.1002/rra.904

Davies-Colley, R. J., Payne, G. W., & Van Elswijk, M. (2000). Microclimate gradients across a forest edge [Article]. *New Zealand Journal of Ecology*, *24*(2), 111-121. https://www.scopus.com/inward/record.uri?eid=2-s2.0-0033828050&partnerID=40&md5=6a2a5ba6cc2d5e5142cb0616acf9c8cd

DNRME. (2019). *Condamine–Balonne Water Resource Plan. . Department of Natural Resources, Mining and Energy, Queensland Government. April 2019*.

Doyle, K., Vu, A. V., Rolfe, Z., & Baumgartner, L. J. (2023). *Menindee Lakes and Darling River Preliminary Water and Sediment Quality Assessment 2023*.

DPIE. (2020). *Water quality technical report for the Intersecting Streams surface water resource plan area (SW13)*.
Durrant-Whyte, H. (2023). *Independent review into the 2023 fish deaths in the Darling-Baaka River at Menindee*.
Ebersole, J. L., Liss, W. J., & Frissell, C. A. (2003). Cold water patches in warm streams: Physicochemical characteristics and the influence of shading [Article]. *Journal of the American Water Resources Association*, *39*(2), 355-368. https://doi.org/10.1111/j.1752-1688.2003.tb04390.x
Facey, J., Balzer, M., Brooks, A., Westhorpe, D., Williamson, N., & Mitrovic, S. M. (2021). *Minimising persistent thermal stratification and algal blooms using improved flow velocity and discharge targets* (Project 08.5 Report). N. D. o. P. a. Environment.
Hodges, K. (2018). *Water quality during lower Balonne larval fish study. Unpublished raw data provided by K. Hodges July 2023*.
Hou, D., He, J., Lü, C., Sun, Y., Zhang, F., Otgonbayar, K. (2013). Effects of environmental factors on nutrients release at sediment-water interface and assessment of trophic status for a typical shallow lake, northwest China. *Scientific World Journal*, 716342. https://doi.org/10.1155/2013/716342
Isaak, D. J., Wollrab, S., Horan, D., & Chandler, G. (2012). Climate change effects on stream and river temperatures across the northwest U.S. from 1980-2009 and implications for salmonid fishes [Article]. *Climatic Change*, *113*(2), 499-524. https://doi.org/10.1007/s10584-011-0326-z
Kaushal, S. S., Likens, G. E., Jaworski, N. A., Pace, M. L., Sides, A. M., Seekell, D., Belt, K. T., Secor, D. H., & Wingate, R. L. (2010). Rising stream and river temperatures in the United States [Article]. *Frontiers in Ecology and the Environment*, *8*(9), 461-466. https://doi.org/10.1890/090037
Klos, P. Z., & Link, T. E. (2018). Quantifying shortwave and longwave radiation inputs to headwater streams under differing canopy structures [Article]. *Forest Ecology and Management*, *407*, 116-124. https://doi.org/10.1016/j.foreco.2017.10.046
Laboratory, M. H. (2023). *Darling River Flood Mapping Study*.
Mallen-Cooper, M., & Zampatti, B. P. (2020). Restoring the ecological integrity of a dryland river: Why low flows in the Barwon–Darling River must flow [Article]. *Ecological Management and Restoration*, *21*(3), 218-228. https://doi.org/10.1111/emr.12428
Mitrovic, S. M., Hardwick, L., & Dorani, F. (2011). Use of flow management to mitigate cyanobacterial blooms in the Lower Darling River, Australia [Article]. *Journal of Plankton Research*, *33*(2), 229-241. https://doi.org/10.1093/plankt/fbq094
Moon, K., Duff, T. J., & Tolhurst, K. G. (2019). Sub-canopy forest winds: understanding wind profiles for fire behaviour simulation [Article]. *Fire Safety Journal*, *105*, 320-329. https://doi.org/10.1016/j.firesaf.2016.02.005
Neldner, V. J., Wilson, B. A., Dillewaard, H. A., Ryan, T. S., Butler, D. W., McDonald, W. J. F., Richter, D., Addicott, E. P., & Appelman, C. N. (2022). *Methodology for survey and mapping of regional ecosystems and vegetation communities in Queensland. Version 6.0. Updated April 2022. Queensland Herbarium, Queensland Department of Environment and Science, Brisbane.*
Olley, J., Burton, J., Hermoso, V., Smolders, K., McMahon, J., Thomson, B., & Watkinson, A. (2015). Remnant riparian vegetation, sediment and nutrient loads, and river rehabilitation in subtropical Australia [Article]. *Hydrological Processes*, *29*(10), 2290-2300. https://doi.org/10.1002/hyp.10369
Petrone, K. C., Richards, J. S., & Grierson, P. F. (2009). Bioavailability and composition of dissolved organic carbon and nitrogen in a near coastal catchment of South-Western Australia. Biogeochemistry,
Quinn, J. M., & Wright-Stow, A. E. (2008). Stream size influences stream temperature impacts and recovery rates after clearfell logging [Article]. *Forest Ecology and Management*, *256*(12), 2101-2109. https://doi.org/10.1016/j.foreco.2008.07.041
Roff, A., Day, M., Thonell, J., & B., D. (2022). NSW State Vegetation Type Map: Technical Notes, NSW Department of Planning and Environment, Parramatta, Australia.

Rutherford, J. C., Blackett, S., Blackett, C., Saito, L., & Davies-Colley, R. J. (1997). Predicting the effects of shade on water temperature in small streams [Article]. *New Zealand Journal of Marine and Freshwater Research*, *31*(5), 707-721. https://doi.org/10.1080/00288330.1997.9516801

Sheldon, F., Barma, D., Baumgartner, L. J., Bond, N., Mitrovic, S. M., & Vertessy, R. (2022). Assessment of the causes and solutions to the significant 2018-19 fish deaths in the Lower Darling River, New South Wales, Australia [Article]. *Marine and Freshwater Research*, *73*(2), 147-158. https://doi.org/10.1071/MF21038

Sweeney, B. W., & Newbold, J. D. (2014). Streamside forest buffer width needed to protect stream water quality, habitat, and organisms: A literature review [Article]. *Journal of the American Water Resources Association*, *50*(3), 560-584. https://doi.org/10.1111/jawr.12203

Tibby, J., Marshall, J. C., Lobegeiger, J. S., Amos, K. J., Pickering, G., & Myburgh, T. (2023). Sedimentation from landscape clearance-induced soil erosion threatens waterhole persistence in a semi-arid river system, southern Queensland, Australia [Article]. *Marine and Freshwater Research*, *74*(12), 1050-1070. https://doi.org/10.1071/MF23016

Townsend, S. A., & Edwards, C. A. (2003). A fish kill event, hypoxia and other limnological impacts associated with early wet season flow into a lake on the Mary River floodplain, tropical northern Australia [Article]. *Lakes and Reservoirs: Science, Policy and Management for Sustainable Use*, *8*(3-4), 169-176. https://doi.org/10.1111/j.1440-1770.2003.00222.x

Vertessy, R., Barma, D., Baumgartner, L. J., Mitrovic, S. M., Sheldon, F., & Bond, N. (2019). *Independent assessment of the 2018-19 fish deaths in the lower Darling*.

Vithana, C. L., Sullivan, L. A., & Shepherd, T. (2019). Role of temperature on the development of hypoxia in blackwater from grass [Article]. *Science of the Total Environment*, *667*, 152-159. https://doi.org/10.1016/j.scitotenv.2019.02.386

Winslow, L., Read, J., Woolway, R., Brentrup, J., Leach, T., Zwart, J., Albers, S., & Collinge, D. (2022). *Package 'rLakeAnalyzer'*. In

Zahraeifard, V., & Deng, Z. (2012). Modeling sediment resuspension-induced DO variation in fine-grained streams [Article]. *Science of the Total Environment*, *441*, 176-181. https://doi.org/10.1016/j.scitotenv.2012.09.059

Zhai, S. Y., Huang, P., Marshall, J. C., Lobegeiger, J., Cramp, R. L., Parisi, M. A., Franklin, C. E., Prior, A., Kurucz, K., & Hipsey, M. R. (2022). *Between a hot place and hypoxia: Modelling fish-kill risk in Queensland waterholes. Report prepared for the Queensland Water Modelling Network, Department of Environment and Science, Queensland Government, Brisbane, Australia.*

Zhai, S. Y., Huang, P., Marshall, J. C., Lobegeiger, J., Cramp, R. L., Parisi, M. A., Franklin, C. E., Prior, A., Kurucz, K., & Hipsey, M. R. (2023). Modelling prolonged stratification and hypoxia in dryland river waterholes during drought conditions [Article]. *Inland Waters*. https://doi.org/10.1080/20442041.2023.2213629